Final Report

Title: Tomographic PIV Study of the Low Re Number Flow Around a Pitching Plate with a Ramp Time History

Principal Investigator: Professor Julio Soria
Department of Mechanical and Aerospace Engineering
Monash University (Clayton Campus)
Melbourne, VIC 3800

Contract Number: FA2386-09-1-4091
AFOSR/AOARD Reference Number: AOARD-09-4091
AFOSR/AOARD Program Manager: Lt. Col John Seo
Period of Performance: 1 Aug 2009 – 3 Sept 2010
Submission Date: 10 Oct 2010

Report Documentation Page

Form Approved
OMB No. 0704-0188

1. REPORT DATE	2. REPORT TYPE	3. DATES COVERED
14 OCT 2010	**Final**	**01-08-2009 to 01-09-2010**

4. TITLE AND SUBTITLE
Tomographic PIV Study of the Low Re Number Flow Around a Pitching Plate with a Ramp Time History

5a. CONTRACT NUMBER
FA23860914091

5b. GRANT NUMBER

5c. PROGRAM ELEMENT NUMBER

6. AUTHOR(S)
Julio Soria

5d. PROJECT NUMBER

5e. TASK NUMBER

5f. WORK UNIT NUMBER

7. PERFORMING ORGANIZATION NAME(S) AND ADDRESS(ES)
Monash University,PO 31, Clayton Campus, Wellington Road,Melbourne, VIC 3800,Australia,NA,NA

8. PERFORMING ORGANIZATION REPORT NUMBER
N/A

9. SPONSORING/MONITORING AGENCY NAME(S) AND ADDRESS(ES)
AOARD, UNIT 45002, APO, AP, 96338-5002

10. SPONSOR/MONITOR'S ACRONYM(S)
AOARD

11. SPONSOR/MONITOR'S REPORT NUMBER(S)
AOARD-094091

12. DISTRIBUTION/AVAILABILITY STATEMENT
Approved for public release; distribution unlimited

13. SUPPLEMENTARY NOTES

14. ABSTRACT

Unsteady aerodynamics in the low Reynolds number domain is of great interest in applications to Micro Air Vehicles (MAVs), especially with respect to flow over, and in the wake of, pitching airfoils. The massively separated flow over the upper surface of the pitching aerofoil allows for the production of large transient peaks of lift at this scale. This study extends our previous work to multi-dimensional (3D), multi-component (3C) measurements of this phenomenon by using Tomographic Particle Image Velocimetry (Tomo-PIV). For this purpose the three-component, three-dimensional (3C-3D) velocity fields in the wake of a flat plate undergoing a pitch-hold-return motion is investigated. The experiments are conducted in a water tunnel at a Reynolds number of 7,500 and a dimensionless pitching rate of Kc = 0.93. The instantaneous and phase averaged evolution of the trailing edge vortices is investigated, highlighting the three-dimensional organization of the coherent vortex structure and its spanwise variation. These experiments represent the first effort in the 3C-3D velocity field mapping of a flat plate undergoing a pitch-hold-return motion. Further optimization of the Tomo-PIV experiments is necessary to extract the full details of the complex vortical flow structure. It has become apparent from this study that the three dimensional flow structure observed in this nominally 2D ?infinite? flat plate is quite different to flow visualizations of unsteady flapping airfoil of low aspect ratio, which suggests that the more relevant case of a low aspect ratio flat plate undergoing a pitch-hold-return motion is a more relevant candidate for a Tomo-PIV study and should be pursued in any future investigation.

15. SUBJECT TERMS
Fluid Mechanics, Tomography, low Reynolds Number

16. SECURITY CLASSIFICATION OF:			17. LIMITATION OF ABSTRACT	18. NUMBER OF PAGES	19a. NAME OF RESPONSIBLE PERSON
a. REPORT **unclassified**	b. ABSTRACT **unclassified**	c. THIS PAGE **unclassified**	**Same as Report (SAR)**	**29**	

Standard Form 298 (Rev. 8-98)
Prescribed by ANSI Std Z39-18

Objectives:
In this study the canonical wall-to wall geometry of a flat plate with rounded leading and trailing edge and pitching motion defined by the AIAA Fluid Dynamics Technical Committee's "Low Reynolds Number Aerodynamics Discussion Group", chaired by Dr. Michael OL of AFRL Air Vehicles Directorate, is employed. This unsteady pitching plate problem is "classical" in the sense of being comparable to results in the literature, but prescribes very high dimensionless transient rates and low Reynolds number, which makes the results applicable to MAVs and pushes the current state of the knowledge and measurement technology through new and unique velocity field measurements. Specifically the objectives of this 12 month study were to:

1. Develop and optimize the optical tomographic recording geometry; develop and implement the 3D tomographic calibration target; determine tomographic reconstruction precision and experimental uncertainty.
2. Set-up and calibrate tomographic PIV (Tomo-PIV) to measure instantaneous 3C-3D flow field of pitching motion.
3. Perform phase-locked Tomo-PIV image data acquisition of low Reynolds Number flow around a pitching plate with a ramp time history.
4. Perform Tomo-PIV image reconstruction and 3C-3D PIV analysis of the 3D reconstructed particle data to extract 3C-3D velocity fields.

Status of effort:
The objectives stated above were achieved and the results of this study have been reported in three conference papers. However, this study also found that the flow adjacent to the surface of the pitching plate was exceedingly difficult to measure with Tomo-PIV with acceptable accuracy. The main reason for this lack of success in applying Tomo-PIV to the measurement of flow adjacent to moving walls it the limited optical recording geometries that are possible in water tunnel based experiments due to the necessity to use large prisms to minimize distortions which a re a consequence of the water –perspex-air interface. Nevertheless, the 3D instantaneous wake structure is amenable to 3C-3D Tomo-PIV measurements and the majority of the effort was channeled toward this aspect of the transient ramp pitching motion of the flat plate. The details of these studies can be found in the three papers attached to this report.

Abstract:
Unsteady aerodynamics in the low Reynolds number domain is of great interest in applications to Micro Air Vehicles (MAVs), especially with respect to flow over, and in the wake of, pitching aerofoils. The massively separated flow over the upper surface of the pitching aerofoil allows for the production of large transient peaks of lift at this scale. This study extends our previous work to multi-dimensional (3D), multi-component (3C) measurements of this phenomenon by using Tomographic Particle Image Velocimetry (Tomo-PIV). For this purpose the three-component, three-dimensional (3C-3D) velocity fields in the wake of a flat plate undergoing a pitch-hold-return motion is investigated. The experiments are conducted in a water tunnel at a Reynolds number of 7,500 and a dimensionless pitching rate of $K_c = 0.93$. The instantaneous and phase averaged evolution of the trailing edge vortices is investigated, highlighting the three-dimensional organisation of the coherent vortex structure and its spanwise variation. These experiments represent the first effort in the 3C-3D velocity field mapping of a flat plate undergoing a pitch-hold-return motion. Further optimization of the Tomo-PIV experiments is necessary to extract the full details of the complex vortical flow structure. It has become apparent from this study that the three-dimensional flow structure observed in this nominally 2D "infinite" flat plate is quite different to flow visualizations of unsteady flapping airfoil of low aspect ratio, which suggests that the more relevant case of a low aspect ratio flat plate undergoing a pitch-hold-return motion is a more relevant candidate for a Tomo-PIV study and should be pursued in any future investigation.

Personnel Supported:
The following personnel was supported by this contract:

Research Fellow: Dr N.A. Buchmann
PhD Student: Mr A-J Buchner, K. Kilaney

The following personnel participated significantly in the research effort:

PhD Student: Mr. C. Atkinson

Publications:

The following paper was peer-reviewed:

- A-J. Buchner, N. A. Buchmann and J. Soria (2010) Wake Measurements of a Pitching Plate using Multi-component, Multi-dimensional PIV Techniques. Proceedings of 17th Australasian Fluid Mechanics Conference, Auckland, New Zealand, 5-9 December 2010.

The following paper was an invited paper:

- N.A. Buchmann, A-J. Buchner, K. Kilany, C. Atkinson and J. Soria (2010) Multi-component, Multi-dimensional PIV Measurements of a Flat-Plate Pitching Motion. AIAA-2010-4278, 40th Fluid Dynamics Conference and Exhibit, Chicago, Illinois, June 28-1, 2010.

The following paper was accepted based on peer-reviewed abstract:

- A-J. Buchner, N. Buchmann, C. Atkinson and J. Soria (2010) 3C-3D Velocity Field Measurements of the Wake Region of Low Reynolds Number Flow around a Flat Plate Undergoing Transient Pitch-Ramp Motion. International Conference on Intelligent Unmanned Systems, Nov 3 - 5, 2010 Bali, Indonesia.

Interactions:

The research conducted with the support of this grant has been presented at the following international conference:

- 40th Fluid Dynamics Conference and Exhibit, Chicago, Illinois, June 28-1, 2010,

and will be presented at the following forthcoming international conferences:

- International Conference on Intelligent Unmanned Systems, Nov 3 - 5, 2010 Bali, Indonesia,
- 17th Australasian Fluid Mechanics Conference, Auckland, New Zealand, 5-9 December 2010.

In addition the results of this study have formed part of the discussion of the AIAA FDTC low-Re discussion group meeting held during the 40th Fluid Dynamics Conference and Exhibit, Chicago, Illinois, June 28-1, 2010.

Inventions:

None:

Archival Documentation:

Attached are copies of:

1. N.A. Buchmann, A-J. Buchner, K. Kilany, C. Atkinson and J. Soria (2010) Multi-component, Multi-dimensional PIV Measurements of a Flat-Plate Pitching Motion. AIAA-2010-4278, 40th Fluid Dynamics Conference and Exhibit, Chicago, Illinois, June 28-1, 2010.
2. A-J. Buchner, N. Buchmann, C. Atkinson and J. Soria (2010) 3C-3D Velocity Field Measurements of the Wake Region of Low Reynolds Number Flow around a Flat Plate Undergoing Transient Pitch-Ramp Motion. International Conference on Intelligent Unmanned Systems, Nov 3 - 5, 2010 Bali, Indonesia.
3. A-J. Buchner, N. A. Buchmann and J. Soria (2010) Wake Measurements of a Pitching Plate using Multi-component, Multi-dimensional PIV Techniques. Proceedings of 17th Australasian Fluid Mechanics Conference, Auckland, New Zealand, 5-9 December 2010.

Multi-component, Multi-dimensional PIV Measurements of a Flat-Plate Pitching Motion

N.A. Buchmann[1], A-J. Buchner[‡], K. Kilany[‡], C. Atkinson[‡] and J. Soria.[2]

Laboratory for Turbulence Research in Aerospace and Combustion (LTRAC)
Department of Mechanical and Aerospace Engineering
Monash University (Clayton Campus), Melbourne, VIC, AUSTRALIA

Unsteady aerodynamics in the low Reynolds number domain is of great interest in applications to Micro Air Vehicles (MAVs), especially with respect to flow over, and in the wake of, pitching aerofoils. The massively separated flow over the upper surface of the pitching aerofoil allows for the production of large transient peaks of lift at this scale. This paper extends our previous work[1] to multi-dimensional (3D), multi-component (3C) measurements of this phenomenon by using Tomographic Particle Image Velocimetry (Tomo-PIV). For this purpose the three-component, three-dimensional (3C-3D) velocity fields in the wake of a flat plate undergoing a pitch-hold-return motion is investigated. The experiments are conducted in a water tunnel at a Reynolds number of 7,500 and a dimensionless pitching rate of K_c = 0.93. The instantaneous and phase averaged evolution of the trailing edge vortices is investigated, highlighting the three-dimensional organisation of the coherent vortex structure and its spanwise variation.

I. Nomenclature

U_∞	=	Free-stream velocity
c	=	Chord of pitching plate
ν	=	Kinematic viscosity
ρ	=	Density
Re	=	Reynolds number, $Re = U_\infty c/\nu$
θ	=	Pitch angle
$d\theta/dt$	=	Pitch rate or angular velocity
K_c	=	Non-dimensional angular velocity ratio, $K_c = d\theta/dt\ c/2U_\infty$
t	=	Time
T	=	Motion period, $T = 1$ second

II. Introduction

THIS paper presents the experimental method and results of an investigation into the canonical problem of a flat plate pitching about the half-chord position in a low Reynolds number flow. Understanding of unsteady and transient aerodynamics has, in the past, been mainly applied to manoeuvre and gust response as well as dynamic stall. Previously, these applications have dictated investigations primarily to high Reynold's number domains (i.e., $>10^6$). However, more recently there have been efforts in extending this knowledge of transient aerodynamics to the low Reynolds number regime for application in biomimetic inspired Micro Air Vehicle (MAV) concepts. Previous work[2-5] has concluded that at small scales it becomes necessary to use separation induced leading edge vortices in the production of lift and thrust. They have further shown that vortices are produced readily via either a pitching or heaving motion of the lifting surface, or a combination of the two movements. For example, such a pitch-heave motion was observed to increase propulsion efficiency of swimming fish by up to 85%[2].

[1] Research Fellow, LTRAC, Dept. of Mech. And Aerospace Eng., Monash Univ, VIC, AUS, AIAA Member
[‡] Graduate Research Student, LTRAC, Dept. of Mech. And Aerospace Eng., Monash Univ, VIC, AUS, AIAA Student Member
[2] Professor, LTRAC, Dept. of Mech. And Aerospace Eng., Monash Univ, VIC, AUS, AIAA Member

Under these rapidly transient conditions, conventional aerodynamic models are no longer applicable and the current understanding of the unsteady phenomena in such flows is limited. For example, the relative importance of coherent motion in the structure and dynamic of these flows remains still unclear. To overcome these difficulties, a suitable canonical problem is investigated in the form of a linear pitch-hold return motion of a flat plate with rounded edges and infinite span. At high dimensionless pitching rates and low Reynolds numbers, this problem is applicable to MAVs, as well as being a 'classical' problem, in the sense that it can be compared to results from literature.

Flow around a flat plate has been studied extensively in the past. At zero angle of attack, the wake formed behind the body assumes a symmetrical time-averaged mean pattern, with the instantaneous flow being characterised by periodic coherent patterns resulting from vortex shedding[6]. In these cases, flow separation occurs at the leading and trailing edge, with two alternating shear layers of opposite sign rolling up into large scale vortices, which are shed into the wake in form of a vortex street.

Early experiments investigating the effect of time varying pitching motion reported the production of a normal force vector with fluctuating thrust and lift components depending on the instantaneous angle of attack[2]. Furthermore, Ol[5] investigated the sensitivity of leading and trailing edge vortex structures to variations in pitch pivot point, and pitch rate. The former was found to have a significant effect mainly on the formation of the leading edge vortex and its size while the latter tends to produce a tighter leading edge vortex if increased. Furthermore, at higher dimensionless pitch rates, a counter-rotating vortex pair dominates the trailing edge vortex structure whilst at lower rates the flow field tends to exhibit a stream of smaller vortices with less domination by any particular structures. Both the trail of smaller vortices, and the larger counter-rotating pair were also observed in the stereoscopic PIV investigation of Kilany et.al.[1]. Under these conditions the leading edge vortex has a tendency to be more diffused and of lower peak vorticity than an equivalent vortex produced at the trailing edge at the same axial location[8].

A. Multi-component, Multi-dimensional Measurement Techniques

This paper extends the work of Kilany et al.[1] to investigating the three-dimensional, three-component (3C-3D) velocity field in the wake of a flat plate undergoing a rapid pitching motion. With the advent of non-invasive, instantaneous whole-field measurement techniques such as Particle Image Velocimetry (PIV), it is now possible to conduct detail 3C-3D measurements of the flow field around the pitching plate and the production of leading and trailing edge vortices.

In the past, several methods have been proposed to obtain a three-dimensional version of the PIV techniques and are extensively reviewed by Arroyo and Hinsch[9]. One technique that enjoys wide popularity is Stereo-PIV[10] as it readily facilitates the measurement of the three-component velocity field on a single plane (3C-2D). While the 3C-2D Stereo-PIV system only provides six of the nine components of the velocity gradient tensor necessary for a complete description of the flow field, it can be extend to a full 3C-3D system by multi-plane Stereo-PIV[11] or a scanning light sheet (SLS) technique[12]. The relatively simple experimental setup, typically composed of a continuos laser light source, a rotating prism for the scanning mechanisms and a high-speed CMOS camera have lead to range of application of this techniques in the past. Although, the SLS allows high in-plane resolution, the method performs best for relatively slow flows and as such is mainly used in water flow applications with velocities below 100*mm/s*.

An instantaneous measurement of the 3D particle motion by means of digital imaging can for example be obtained by 3D Particle Tracking Velocimetry (PTV)[13] or defocusing PIV[14]. Both of these methods require the detection of individual particle images in the 3D object space, which with the current algorithms can be performed accurately, but only for a relatively low particle concentration, thus limiting the spatial resolution of these methods. Another technique suitable for 3C-3D PIV measurements is tomographic digital in-line holography[15] which is well suited for high spatial resolutions, but limited to small measurement domains due to the limited size of the digital recording array.

A more recent and increasingly popular 3C-3D technique is tomographic PIV (Tomo-PIV)[16]. This method does not require the detection of individual particles and is based on the simultaneous recording of the illuminated seeding particles within a 3D light volume along several observation directions similar to stereo-PIV. The recorded light intensity distribution is reconstructed over a three-dimensional array of voxels, yielding the three-dimensional

light distribution, which is analogue to the traditional digital PIV image. The 3D light volume is then analysed by means of 3D cross-correlation to determine the corresponding 3C-3D instantaneous velocity field over the entire measurement volume.

III. Principle of Tomographic PIV

This section gives a brief overview of the tomographic PIV technique and the volume reconstruction technique used in this work. A more complete description of the Tomo-PIV technique is available in Elsinga et al.[16] and Atkinson and Soria[17]. In Tomo-PIV, the seeded flow is illuminated with a thick laser light sheet and the 3D intensity distribution of the tracer particles is determined and subsequently cross-correlated to yield the 3C-3D velocity field. This process requires the reconstruction of the 3D intensity distribution from multiple instantaneous camera views via algebraic tomographic reconstruction techniques as illustrated in Figure 1. To date, the most commonly used technique is the multiplicative algebraic reconstruction technique (MART)[16], which is well suited for the limited number of views typically available in fluid experiments and compared with other algebraic reconstruction techniques, provides better reconstruction quality in fewer iterations[18]. However, the MART algorithm requires long reconstruction times and large computer memory allocations, which to some extent impede the application of Tomo-PIV as a routine tool for experimental investigations

For example, the number and size of the reconstructed volumes is generally limited by the computational demand and storage required to perform each reconstruction. Reconstructions times for a single volume of 730 × 730 × 184 voxels, using the MART algorithm have been quoted at approximately 1h of computer processing time per volume object[19], while reconstruction of larger volumes (e.g., 3,512 × 2,562 × 500 voxel) can require up to 34h on a single dual-core processor[20]. For 16-bit intensity fields, this corresponds to reconstructed volume file sizes in the order of 200 MB and 10 GB for small and larger volumes, respectively. This imposes a significant restriction on the applications of Tomo-PIV in terms of data processing and storage and typically limits Tomo-PIV to low resolutions and small sample sizes.

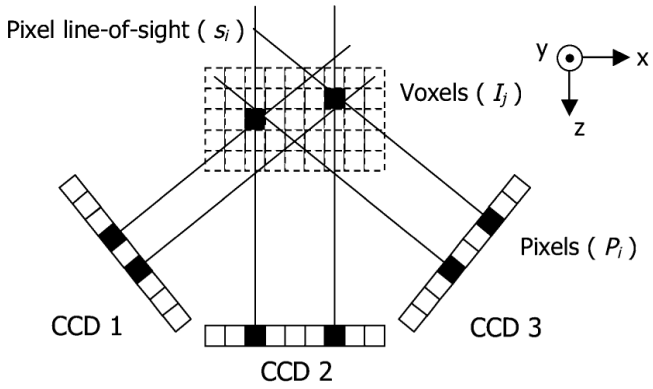

Figure 1. Schematic of multi-camera algebraic reconstruction technique used in Tomo-PIV. Filled voxels represent particle locations required to satisfy the filled pixels in each CCD recorded projection.

A. MLOS-SMART Technique

An alternative and more time efficient method to the above MART reconstruction is the multiplicative line-of-sight simultaneous multiplicative reconstruction technique (MLOS-SMART) proposed by Atkinson and Soria[17]. Considering that for a typical PIV experiment only 10-15 particle pairs per interrogation region are sufficient to obtain a valid displacement estimate[21], the resulting volume fraction of the reconstructed particles is less than 5%. This means that approximately 95% of the reconstructed volume will have a negligible intensity and can be excluded from the reconstruction process, thus reducing computational and data storage requirements. The MLOS-SMART technique takes advantage of this concept via a multiplicative line of sight (MLOS) approach to isolate the expected non-zero points from the reconstruction volume. This results in an initial estimate of the 3D particle intensity distribution, which contains the approximated particle intensities, but also ghosts particles due to the non-

uniqueness of the camera projections. In order to reduce the intensity of the ghost particles, the MLOS estimation is followed by an iterative voxel correction in the form of the simultaneous multiplicative algebraic reconstruction technique (SMART), which is only performed on the non-zero voxels. The SMART technique is based on the same principles as the MART technique and the only difference is the method by which the correction is determined (see Atkinson and Soria[17] for more details). Following the volume reconstruction, the 3D particle intensity fields are evaluated with a 3D spatial cross-correlation routine[22] to determine the instantaneous 3C-3D velocity fields.

The most important limiting factors in Tomo-PIV are the extent of the measurement volume in the third direction (i.e., depth) and the required laser power for volume illumination, which can be 5-10 times larger than for a stereo-PIV experiment. Furthermore, the accuracy of the reconstruction process depends upon several factors among which the most important are the number of independent viewing directions and the particle seeding density. Simulations by Atkinson and Soria[17] for a 4 camera Tomo-PIV setup with a 0.05 particle per pixel *(ppp*) seeding density, show an acceptable accuracy of the MLOS-SMART technique after 40 iterations compared to the traditionally used MART reconstruction with 5 iterations. Moreover, when using MLOS-SMART, the required reconstruction reduces by almost one magnitude and the total memory requirements reduce by a factor of 15, constituting a significant improvement in computational efficiency.

IV. Experimental Apparatus and Methodology

A. Water Tunnel and Pitching Plate Apparatus

The experiments are conducted in the horizontal water tunnel located at the Laboratory for Turbulence Research in Aerospace and Combustion (LTRAC). The tunnel has a length of approximately 5000*mm* with its cross-section measuring 500*mm* × 500*mm* and is shown schematically in Figure 2(a). The experiments are conducted approximately 4000*mm* downstream of the contraction (10:1) where the free-stream turbulence level is less than 0.5% and the velocity profiles are uniform across the width of the test section[3].

A carbon fibre flat plate with rounded edges, chord length 100*mm*, span 470*mm* and thickness of 2.3*mm* is used for the current experimental investigation. The flat plate is dimensionally similar to that used by Ol[6] and chosen to minimise blockage effects at the maximum pitch angle. The transient pitch-hold-return motion of the flat plate is shown in Figure 3 and characterised by the non-dimensional velocity ratio:

$$K_c = \frac{d\theta}{dt}\frac{c}{2U_\infty} \tag{1}$$

where $d\theta/dt$ is the constant angular velocity of the flat plate, U_∞ the free-stream velocity and c the chord length. The Reynolds number is defined as $Re = U_\infty c/\nu$ and the velocity, length and vorticity scales are non-dimensionalised by the free-stream velocity, the chord length c and the ratio c/U_∞, respectively. A summary of the current experimental parameters is given in Table 1, which are identical to those used previously by Kilany et al. [1].

Table 1. Experimental parameters.

Parameter	Quantity
c	100*mm*
U_∞	75*mm/s*
θ	$0 - 40^\circ$
Re	7,500
K_c	0.93

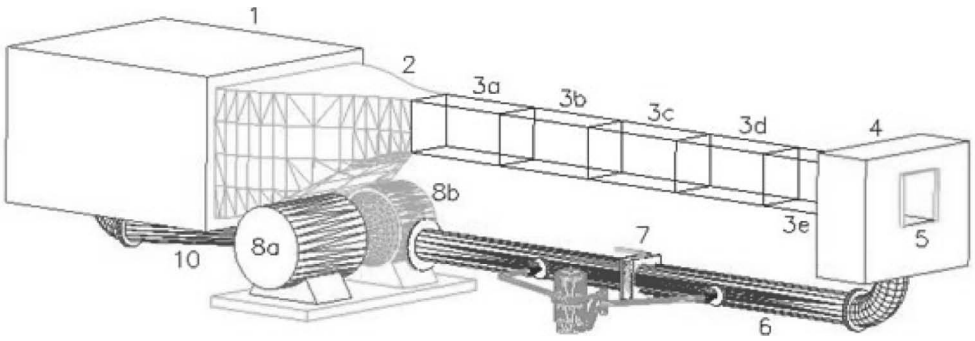

(a)

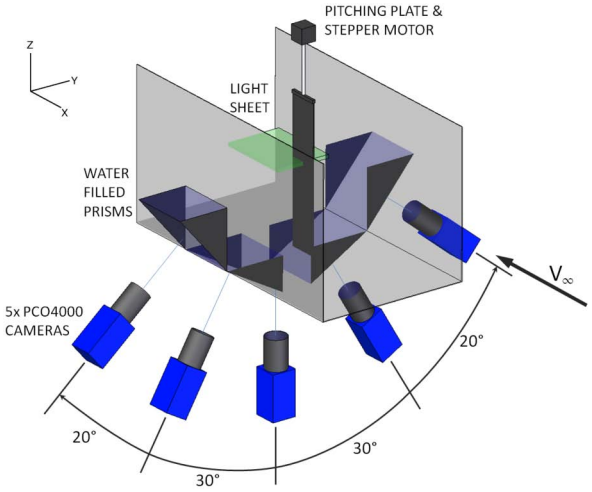

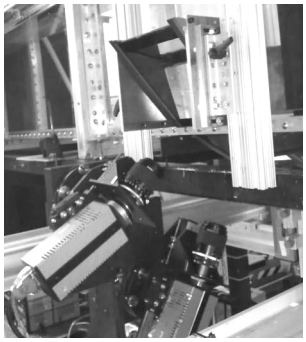

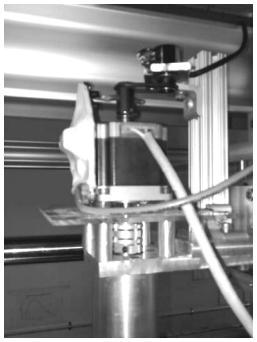

(b) (c) (d)

Figure 2. Experimental Setup: (a) Closed circuit horizontal water tunnel; (b) Schematic of the optical arrangement showing the 5 digital cameras, viewing prisms, measurement volume and flat plate geometry; (c-d) details of the camera setup and pitching mechanism.

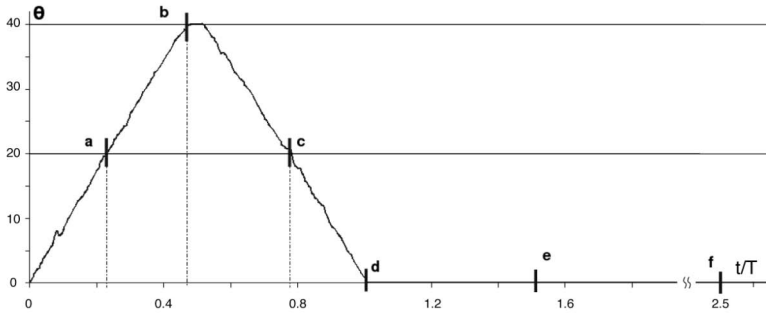

Figure 3. Measured pitch angle of the flat plate as a function of t/T. (a) t/T = 0.24, (b) t/T = 0.47, (c) t/T = 0.77, (d) t/T = 1.0, (e) t/T = 1.5, (f) t/T = 2.5 with T = 1*sec.*

The flat plate pitches around half chord (i.e., $c/2$) and is mounted vertically in the test section as shown in Figure 2(b-d). A coordinate system anchored on the half-chord at mid-span is employed denoting the streamwise, lateral and spanwise direction with x, y and z, respectively. A stepper motor mounted directly above the test section as indicated in Figure 2 generates the pitch-hold-return motion at a resolution of 80,000 steps per revolution with a torque of 1.6*Nm*. The motion of the stepper motor is accurately controlled using an in-house motion control program

stored on a Motion Architect AT6400 multi-axis motor controller. This enables the desired motion sequence to be defined, in which the plate pitches linearly to a maximum pitch angle of $\theta = 40^{\circ}$, holds for 0.05 t/T and returns to its zero position before waiting 20 time periods (T = 1sec) prior to repeating the motion cycle. Figure 3 depicts this motion sequence as measured by the angular displacement encoder mounted at the top of the flat plate.

B. Optical Setup

The 3C-3D measurements are conducted in a volume located at the mid-span of the plate and aligned with the x-y coordinate system. The Tomo-PIV setup consists of five PCO.4000 digital CCD cameras (4008 × 2672 $pixel^2$, 16bit), equipped with 105mm focal length lenses and arranged in an angular configuration of 0°, $\pm 30^{\circ}$ and $\pm 50^{\circ}$ as shown in Figure 2(b). Water filled viewing prisms are attached to the tunnel sidewalls to reduce the optical distortions created by the air –water interface. Additionally, the Scheimpflug condition is imposed for each camera to maximize the image focus throughout the measurement volume. A summary of the Tomo-PIV parameters is given in Table 2.

The flow is seeded with 54μm nylon spheres (ρ = 1.01g/cm^3) and illuminated with a 240mJ pulsed, dual-cavity Nd:YAG laser. A cylindrical diverging lens is used to shape the beam into an approximately 14mm thick light sheet, which is passed through a slit to trim the lower intensities at the edges to provide a more even illumination of the measurement volume. The light sheet is introduced into the test section through a mirror located in the center of the tunnel and downstream of the test section. The time separation, Δt between the two exposures is 6ms yielding a mean particle displacement of approximately 12 $pixel$ or 0.48mm. Due to the lower laser light intensity per unit volume, larger seeding particles are required to provide adequate scattering intensity to each CCD array. The seeding density is adjusted to approximately 0.01ppp and the data acquisition is synchronized to the plates' pitching motion

The cameras are calibrated using the method described by Soloff et al. [23]. A calibration plate consisting of black dots on white background is traversed through the measurement volume from z = -6mm to z = +6mm in steps of 1mm and an uncertainty of 5μm. A volume self-calibration analogous to that of Wieneke[24] is also applied to reduce the calibration error of approximately 10 $pixels$ to below 1 $pixel$.

Table 2. Parameters of the Tomo-PIV system

	Parameter	Quantity
Tomo-PIV setup	Cameras	4008 × 2672 $pixel^2$, 16bit 0°, $\pm 30^{\circ}$ and $\pm 50^{\circ}$
	Laser	Nd:YAG, 240mJ
	Flow seeding	54μm nylon spheres, (ρ = 1.01g/cm^3)
Imaging properties	Magnification	0.26
	Resolution	25 $pixel/mm$
	FoV ($S_x \times S_y \times S_z$)	3500 × 2250 × 350 $pixel^3$ 130 × 90 × 14 mm^3 1.3 × 0.9 × 0.14 c
	Lens aperture (f#)	11
	Particle image diameter	≈ 2.3 $pixel$
	Depth of field	≈ 12mm
	Separation time	5 ms
	Max. displacement	12 pixel

C. Tomographic PIV Analysis

The recorded images are pre-processed to remove the background intensity as required by the MLOS-SMART algorithm and to eliminate background and CCD noise. The image processing involves background subtraction, followed by band-pass filtering and Gaussian smoothing to equalize the particle intensities across the image and between cameras. Subsequently, volume reconstruction is performed with 10 iterative corrections of the MLOS-SMART technique and an initial solution and relaxation parameter of unity. The particle intensities are reconstructed in a volume of size $3500 \times 2250 \times 350 pixel^3$. The corresponding physical dimensions are $130 \times 90 \times 14 mm^3$ (or $1.3 \times 0.9 \times 0.14$ *chords*) with a pixel-to-voxel ratio of approximately 1:1 and a discretisation of 25 *pixel/mm*.

The velocity fields are calculated with an in-house developed multigrid multi-pass FFT-based cross-correlation algorithm[22]. Interrogation volumes of 64^3 voxels (= 2.56*mm*) with 50% overlap are used to provide fields of $98 \times 65 \times 9$ vectors. The calculated vectors are validated with a normalised local median filter[25] and a maximum displacement limit. Invalid vectors are replaced with a mean vector interpolation, which typically account for less than 2% of the total vector count. Prior to the data visualization, the velocity fields are filtered by convolution with a 3×3×3 Gaussian kernel ($\sigma = 1$) to suppress noise fluctuations in the velocity gradients[26,27]. Note that the filter kernel is equal to the interrogation window size and as such the spatial frequency response remains unaffected.

As mentioned before, the procedure involving volume reconstruction and 3D cross-correlation is computationally expensive, requiring approximately 10*h* and 6GB RAM memory for a single instantaneous velocity field on a single core 2.8 MHz Intel processor. The memory required for storing a single volume pair at 16bit amounts to approximately 10GB compared to the initial 140MB of the recorded images. The total memory requirements to reconstruct, analyse and store the 105 instantaneous velocity fields employed in this study are in excess of 1TB. Even though for a small sample size only, this clearly highlights the dramatic increase in processing power and data storage requirements needed for such 3C-3D Tomo-PIV flow studies.

V. Previous Stereoscopic PIV Measurements

To describe the large-scale flow field around the pitching plate this section presents a short summary of our previous stereoscopic PIV measurement and related work under similar flow conditions to those employed in this study (i.e., $K_c = 0.93$, $Re = 7{,}500$). The experimental procedure is similar to that used in this study and a more detailed description can be found in Kilany et al.[1].

Figure 4 provides a comparison of the phase averaged vector fields and spanwise vorticity contours with flow visualization data obtained from Ol[6] for $K_c = 0.7$, $Re = 10{,}000$. As a result of the pitch-up and pitch-down motion, a number of small, counter rotating vortical structures peal off the trailing edge and quickly coalesce into more coherent larger vortices, which are convected downstream. The leading edge vortex is formed during the pitch-down maneuver and travels downstream towards the trailing edge along the upper surface of the flat plate and is mainly responsible for lift production[5]. Although for a slightly different set of flow parameters, the comparison with the flow visualization data reveals a good agreement, particularly for the shear layer and the counter-rotating vortex pairs shed from the trailing edge.

Furthermore, at lower dimensionless pitching rates and Reynolds number ($K_c = 0.2$, $Re = 1{,}000$), Eldredge et. al.[5] observes a merging of the trailing and leading edge vortex regions while at higher dimensionless pitching rates (similar to the one used in this work) more distinctly separate structures are reported. The size and structure of the trailing edge vortices from our previous stereo-PIV also compares favorable with the above work for the range of selected flow parameters.

The novelty of the present work is the extension of the current data set and knowledge base by performing multi-component, multi-dimensional velocity field measurements. Unlike in our earlier stereo-PIV measurements, the geometric considerations required for such a complex multiple camera setup prevented 3C-3D measurement in the direct vicinity of the pitching plate. Therefore, and as a first step towards multi-component, multi-dimensional flow measurements of such complex flows, this work will only study the instantaneous and phase averaged 3C-3D flow structure in the wake of the rapidly pitching plate.

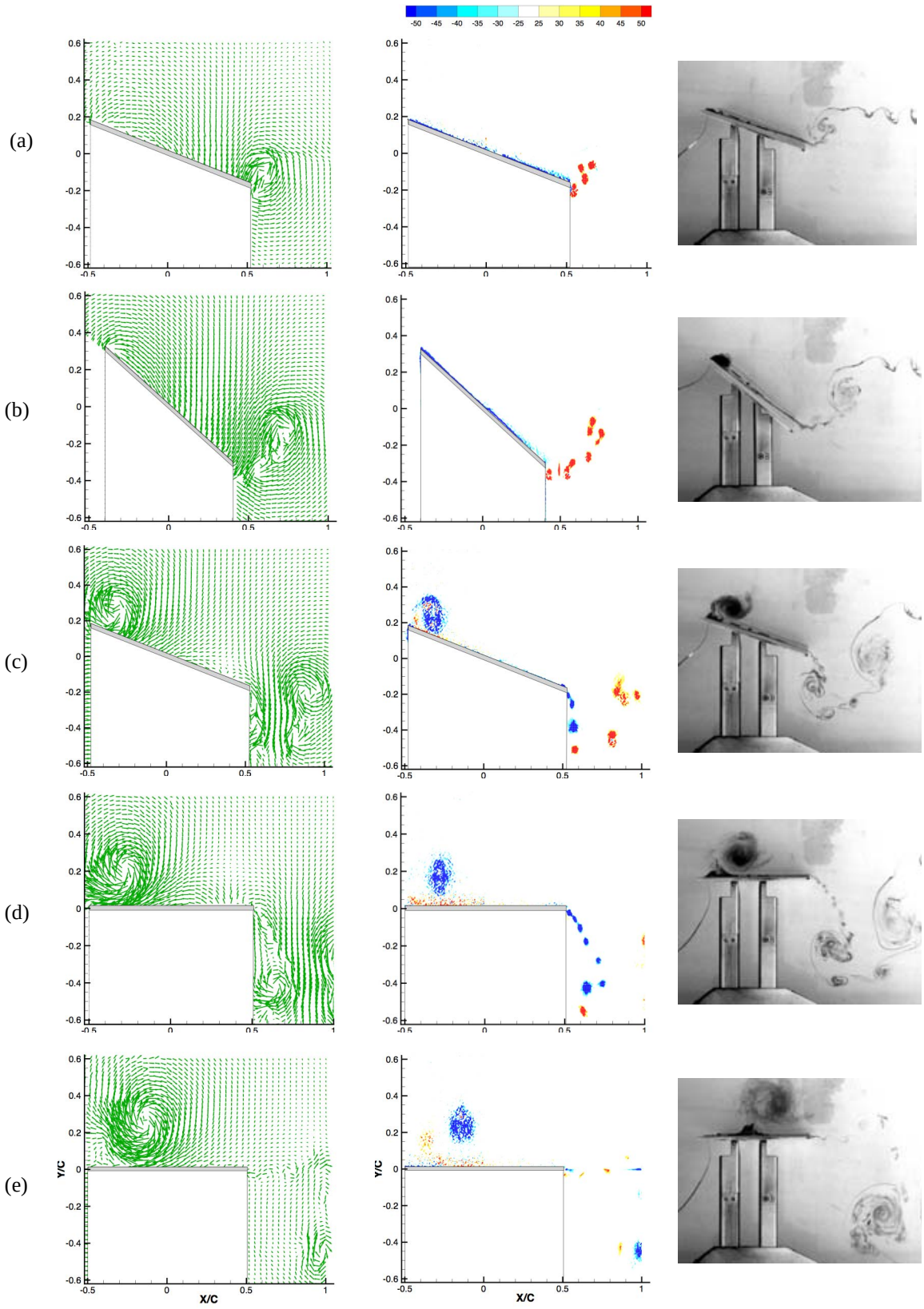

Figure 4. Stereo-PIV results for K_c = 0.93, *Re* = 7,500 (left and middle) and flow visualization results by OI[6], K_c = 0.7, *Re* = 10,000 (right): (a) t/T = 0.22, (b) t/T = 0.47, (c) t/T = 0.77, (d) t/T = 1.0, (e) t/T = 1.5.

VI. Results and Discussion

A. Phase Averages

The extension of the stereo-PIV results into three dimensions allows the observation of spanwise variations in the vortical structures. In the following, phase averaged 3C-3D velocity fields, measured at discrete time steps in the pitch cycle are presented and discussed. Due to computational time limitations, phase averages are only calculated from 15 instantaneous data sets, however further data processing is still ongoing. The phase averaged flow fields are useful in determining the periodic nature of the flow structures, without reference to specific stochastic disturbances

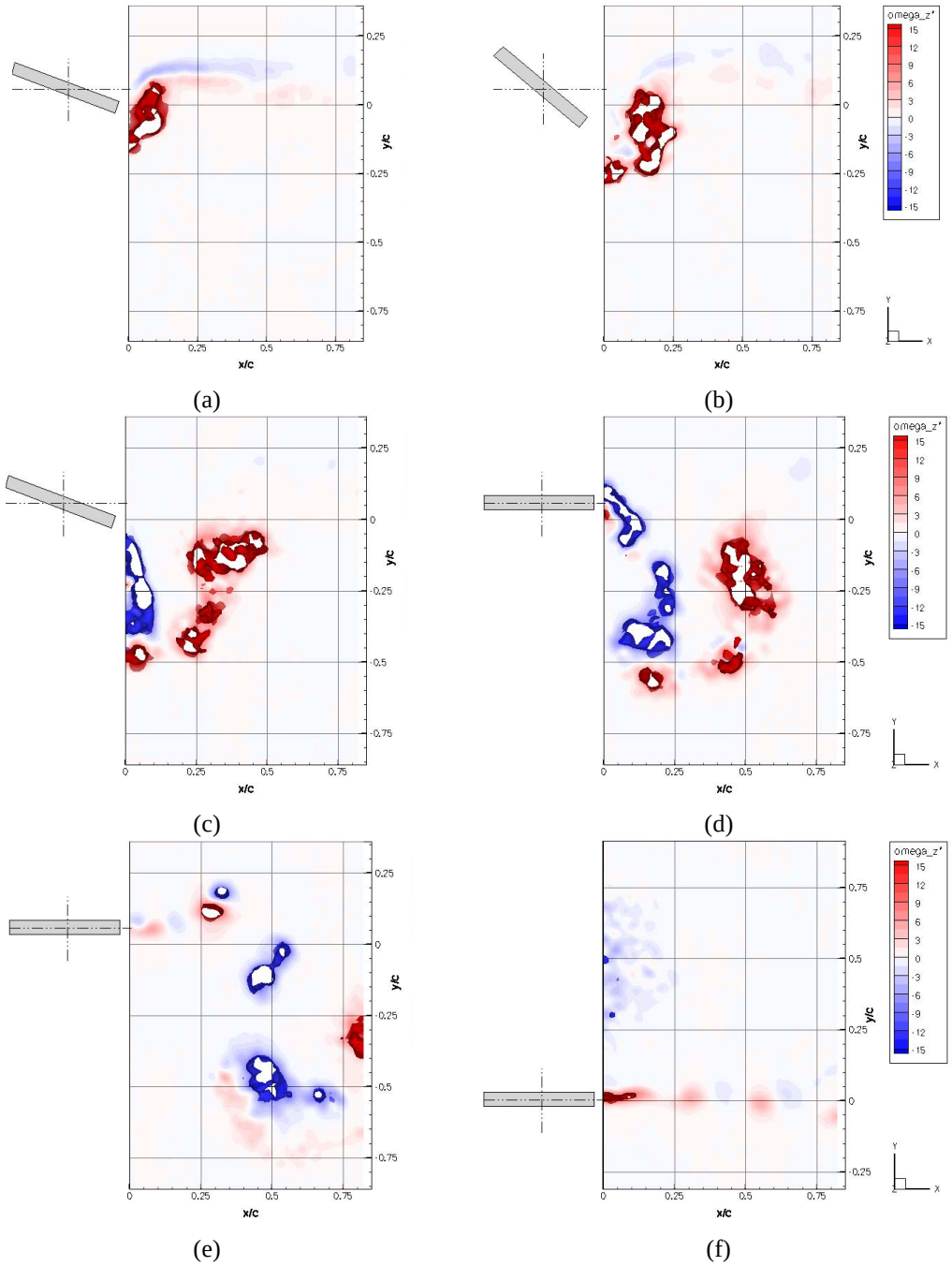

Figure 5. Phase averaged 3C-3D spanwise vorticity fields: (a) t/T = 0.22, (b) t/T = 0.47, (c) t/T = 0.77, (d) t/T = 1.0, (e) t/T = 1.5, (f) t/T = 2.5.

and instabilities within the flow that vary from cycle to cycle. Figure 5 demonstrates the structure of the vortices shed from the plate during the pitching motion in form of 3D vorticity isocontours, projected onto the mid-plane for better comparison.

At $t/T = 0.24$, the angular acceleration of the plate has succeeded in producing a region of positive vorticity at the trailing edge, which are then convected downstream while the trailing edge of the plate continues to produce positive vorticity up until the plate reaches it maximum angle at $t/T = 0.47$. Vortices of opposite sign are produced as the plate rotates back towards its zero position at $t/T = 0.77$ (Fig. 5(c)) and continue to develop until the completion of the motion cycle at $t/T = 1.0$. Consistent with previous observations, the vorticity is generated as a succession of small vortices, which as they convect downstream, coalesce into larger structures (e.g., Fig. 5(e)). At $t/T = 2.5$, the trailing edge structures have moved out of the field of view and the leading edge vortex starts to move into the field of view from the left. This vortex is of significantly larger size, but less intense than the vortices produced at the trailing edge.

The wake in Figure 5(a) is indicative of the averaging process introduced by the phase averaging wherein random structures, which do not occur at each phase, are progressively removed from the dataset. This is particularly apparent at $t/T = 0.24$ where the Karman vortex street shed from the trailing edge prior to the initialization of the motion appears as a steady wake-like structure containing two parallel regions of opposite vorticity. Conversely, after the end of the motion sequence ($t/T = 2.5$, Fig. 5(f)), the Karman vortex street remains despite the phase averaging, which indicates a characteristic periodicity of the redeveloping wake. Upon completion of the motion sequence, the plate always decelerates at the same rate and direction, producing the same sequence of trailing edge vortices. This leads to the development of a unique Karman street that is started under the same initial conditions each time, and therefore the first vortex in the street is shed in the same direction each period. This for example can be seen clearly in Figure 5(e) where the main trailing edge vortices are convected from the trailing edge and the Karman street has begun to form.

The phase averaged flow fields, shown in Figure 5, exhibit the same general behavior as that observed in the stereo-PIV measurements. This confirms the congruency of the experimental setup and flow conditions with those of Kilany et. al.[1] thus validating the direct comparison of observations made from both data sets.

B. 3C-3D Instantaneous Vortex Structure

Instantaneous 3C-3D velocity fields and vorticity iso-contours at $t/T = 0.77$, 1.0 and 2.5 are shown in Figure 6-8 where the mean convection velocity has been subtracted for better visualisation. It can be seen that during the return motion ($t/T = 0.77$, Fig. 6) a significant spanwise velocity exists, which primarily is associated with each of the vortical regions produced at the trailing edge during pitch up and pitch down motions. Furthermore, the streamlines in Figure 6(a) exemplify the actual spiraling motion of the flow in these vortices, a feature that is not readily apparent in stereoscopic PIV and cannot be measured using planar PIV methods. The out of plane, or spanwise, flow induced by these vortices is a feature of "vortex stretching", a necessary phenomenon in order to satisfy continuity and conservation of angular momentum. The stretching occurs as a result of the finite span of the flat plate and the deformation of the vortex tube by the boundary layer flow along the test section walls. The lateral flow (i.e., in the y-direction) between the counter-rotating vortices should also be noted. In these regions, the streamwise velocity equals the free-stream velocity and a significant 'downwash' occurs as a result of the counter-rotating vortices. This effect is also apparent at $t/T = 1.0$, at the conclusion of the motion cycle.

At the completion of the pitching motion ($t/T = 1.0$, Fig. 7), the area of 'downwash' is accompanied by a significant increase in spanwise velocity forming a spiral pattern around and through the trailing edge vortex region. The streamwise flow occurs in both directions and reaches peak values in the order of ±10-15% of the mean convection velocity. It should further be noted that the spanwise velocity component is not constant throughout the thickness of the measurement volume, as seen by the contour levels on the lower, and right-hand edges of the volume.

At $t/T = 2.5$, (Fig. 8), the leading edge vortex has begun to move into the field of view while the trailing edge structures have convected downstream. There are significant variations and small-scale structures within in the leading edge vortex, showing that the instantaneous flow fields contain significant stochastic variation. This

variation occurs not only in-plane but also through the depth of the reconstructed volume. The effect of the convecting leading edge vortex on spanwise motion is less pronounced than that of the trailing edge structures, which is a consequence of the more diffuse nature of this vortex, with lower peak vorticity.

Also, there appears to be a relationship between the peak strength of any particular vortex and the induced spanwise velocity component, but this requires further analysis of the current data sets. Figure 8(b) again demonstrates the constant periodic nature of the trailing edge von Karman street with respect to the pitching motion phase. Lastly, it is important to note that the above observations relate to the instantaneous velocity fields and may differ from phase averaged observations.

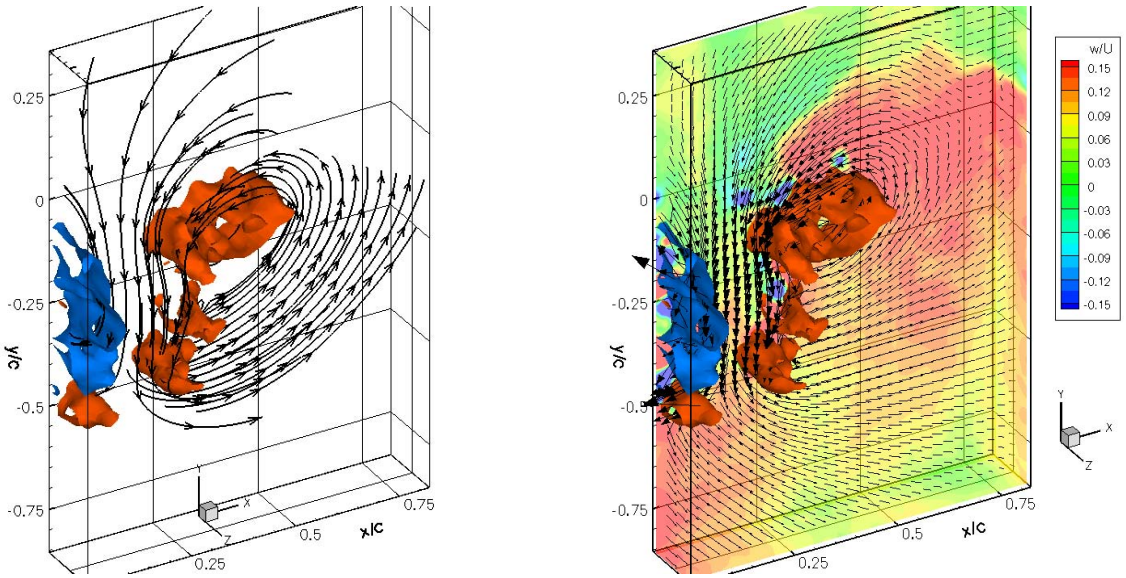

(a) (b)

Figure 6. Instantaneous 3C-3D velocity field at *t/T* = 0.77: (a) Isocontours of spanwise vorticity and selected streamlines and (b) normalised spanwise velocity contours.

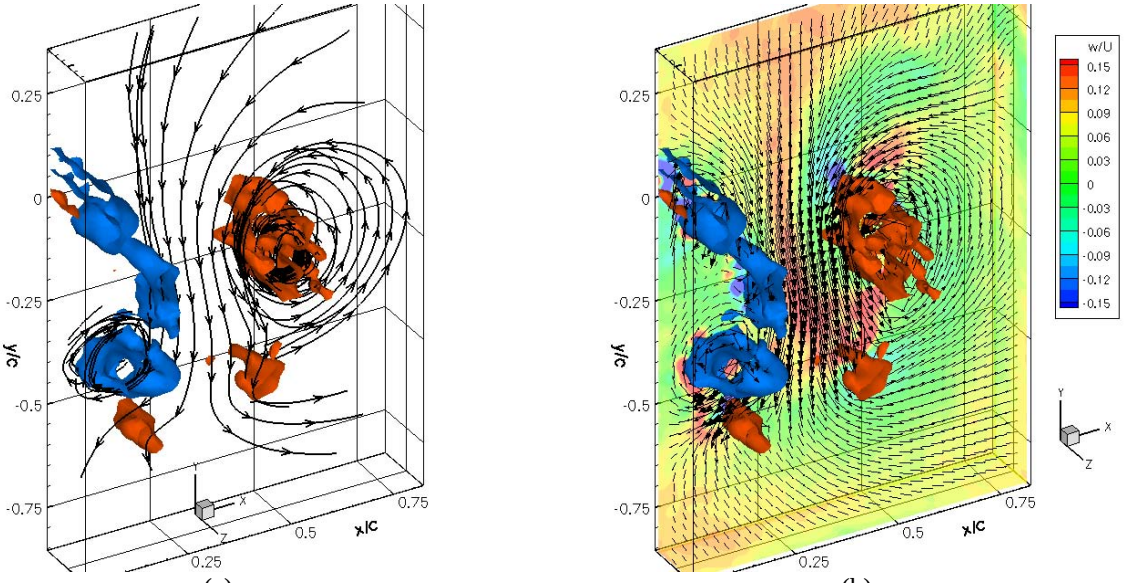

(a) (b)

Figure 7. Instantaneous 3C-3D velocity field at *t/T* = 1.0: (a) Isocontours of spanwise vorticity and selected streamlines and (b) normalised spanwise velocity contours.

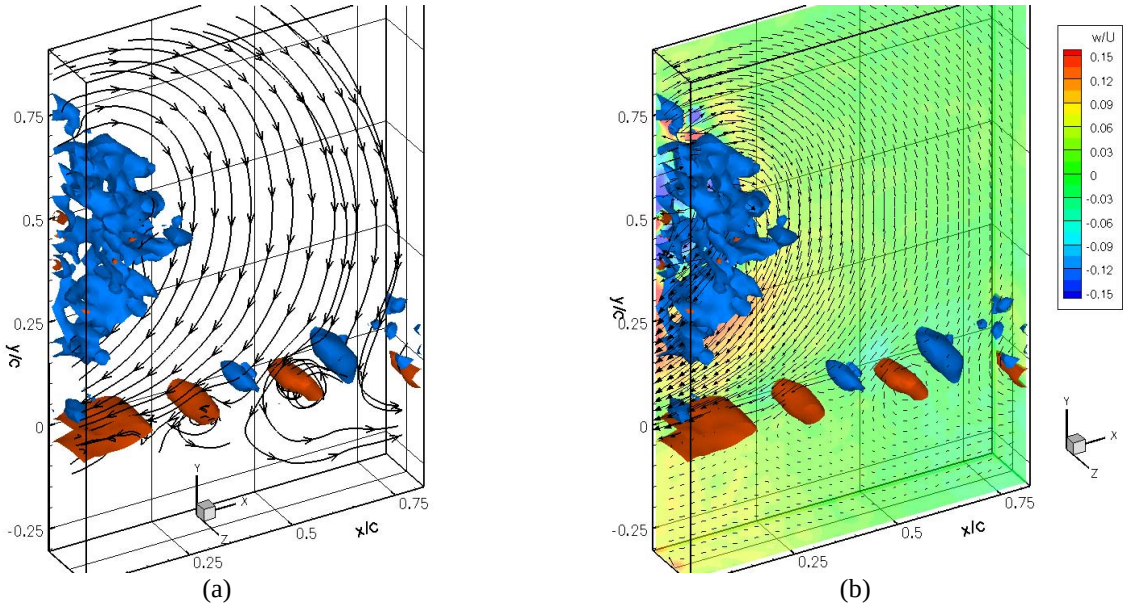

(a) (b)

Figure 8. Instantaneous 3C-3D velocity field at *t/T* = 2.5: (a) Isocontours of spanwise vorticity and selected streamlines and (b) normalised spanwise velocity contours.

VII. Concluding Remarks

Investigations such as those carried out by Parker et. al.[28] show the three-dimensionality of flows past a pitching aerofoil of finite span, but fail to address the existence of three-dimensional structures within the unsteady vortex sheet produced by a nominally infinite oscillating aerofoil. In employing the same motion profile and conditions as Kilany et. al.[1], the results in this paper were directly compared to their 3C-2D stereoscopic PIV data. The flow patterns in the wake of the pitching plate, as observed by Kilany et. al.[1], were shown here to contain significant variation in the spanwise dimension as well as exhibiting a spanwise axial flow component indicative of the presence of vortex stretching as described in Petitjeans and Wesfried[29]. It is interesting to note that even in the early investigation of Koochesfahani[8], coherent spanwise velocity components were observed in the core of the vortices produced by pitching aerofoils and that this axial component varied with both amplitude and frequency of the lifting surface oscillation. In this study it was hypothesised that one of the driving factor behind the phenomenon is the finite length of the aerofoil and the effect of the no-slip boundary condition on the walls of the water tunnel. The 3C-3D flow fields provided by the tomographic PIV methods in the present study show these phenomena qualitatively as well as quantitatively.

In conclusion, this study has provided for the first time preliminary 3C-3D velocity field data of the wake flow behind a flat plate undergoing a rapid pitch-hold-return motion and has proven the general feasibility of conducting Tomo-PIV measurements in such complex flows. The results provided an unprecedented insight into the three-dimensional, coherent flow structure of a rapidly pitching aerofoil and promise great potential for future investigations. However, it should be noted that the computational demands for data processing and particularly data storage currently limit the application of Tomo-PIV as a routine tool. Therefore, future investigations require careful selection of the flow parameters to optimise the required experimental and numerical effort.

Acknowledgments

This material is based on research sponsored by the Air Force Research Laboratory, under grant number FA2386-09-1-4091. The U.S. Government is authorized to reproduce and distribute reprints for Governmental purposes notwithstanding any copyright notation thereon

References

[1]Kilany K., Judde, C., and Soria, S., "Multi-component, Multi-dimensional PIV Measurements of Low Reynolds Number Flow Around Flat Plate Undergoing Pitch-Ramp Motion", *39th AIAA Fluid Dynamics Conference*, San Antonio, Texas, 2009.

[2]Anderson, J. M., Streitlien, K., Barrett, D. S., and Triantafyllou, M. S., "Oscillating foils of high propulsive efficiency", *Journal of Fluid Mechanics*, Vol. 360, 1998, pp. 41-72.

[3]Parker, K., von Ellenrieder, K. D., and Soria, J., "Using stereo multigrid DPIV (SMDPIV) measurements to investigate the vortical skeleton behind a finite-span flapping wing", *Experiments in Fluids*, Vol. 39, 2005, pp. 281-298.

[4]Shyy, W., Lian, Y., Tang, J., Liu, H., Trizila, P., Stanford, B., Bernal, L., Cesnik, C., Friedmann, P., and Ifju, P., "Computational aerodynamics of low Reynolds number plunging, pitching and flexible wings for MAV applications", *Acta Mechanica Sinica*, Vol. 24, 2008, pp. 351-373.

[5]Eldredge, J. D., Chengjie, W., and Ol, M. V., "A computational study of a canonical pitch-up, pitch-down wing maneuver", *39th AIAA Fluid Dynamics Conference*, San Antonio, Texas, 2009.

[6]Ol, M.V., "The High-Frequency, High-Amplitude Pitch Problem: Airfoils, Plates and Wings", *39th AIAA Fluid Dynamics Conference*, San Antonio, Texas, 2009.

[7]Lam, K. M., and Leung, M. Y. H., "Asymmetric vortex shedding flow past an inclined flat plate at high incidence", *European Journal of Mechanics B/Fluids*, Vol. 24, 2005, pp. 33-48.

[8]Koochesfahani, M. M., "Vortical patterns in the wake of an oscillating airfoil", *AIAA Journal*, Vol. 27, 1989, pp. 1200-1205.

[9]Arroyo, M. P. and Hinsch, K. D. (2008). Recent developments of piv towards 3d measurements. In Schr oder, A. and Willert, C., editors, Particle Image Velocimetry: New Developments and Recent Applications. Springer-Verlag Berlin-Heidelberg.

[10]Prasad, A. K., and Adrian, R. J., "Stereoscopic particle image velocimetry applied to liquid flows" *Experiments in Fluids*, Vol. 15, 1993, pp. 49-60.

[11]Ka hler, C. J. (2004). Investigation of the spatio-temporal flow structure in the buffer region of a turbulent boundary layer by means of multiplane stereo piv. Experiments in Fluids, 36(1):114–130.

[12]Burgmann, S., Bru cker, C., and Schro der, W. (2006). Scanning piv measure- ments of a laminar separation bubble. Experiments in Fluids, 41:319–326.

[13]Pereira, F., Stuer, H., Graft, E. C., and Gharib, M. (2006). Two-frame 3d particle tracking. Measurement Science and Technology, 17(7):1680 – 1692. Particle tracking;Two frame;Defocussing;Defocusing digital particle image velocimetry (DDPIV);.

[14]Willert, C. E. and Gharib, M. (1992). Three-dimensional particle imaging with a single camera. Experiments in Fluids, 12(6):353–358.

[15]Soria, J. and Atkinson, C. (2008). Towards 3c-3d digital holographic fluid velocity vector field measurement—tomographic digital holographic piv (tomo-hpiv). Measurement Science & Technology, 19(7).

[16]Elsinga, G. E., Scarano, F., Wieneke, B., and van Oudheusden, B. W. (2006). Tomographic particle image velocimetry. Experiments in Fluids.

[17]Atkinson, C. and Soria, J. (2009). An efficient simultaneous reconstruction technique for tomographic particle image velocimetry. Experiments in Fluids, 47(4):553–568.

[18]Atkinson, C. H. and Soria, J. (2007). Algebraic reconstruction techniques for tomographic particle image velocimetry. In Proceedings of the 16th Australasian Fluid Mechanics Conference, Gold Coast, Australia.

[19]Scarano, F., Elsinga, G., Bocci, E., and van Oudheusden B.W. (2006). In- vestigation of 3-d coherent structures in the turbulent cylinder wake using tomo-piv. in:. In 13th Int. Symp on Applications of Laser Techniques to Fluid Mechanics, Lisbon, Portugal.

[20]Hain, R., Ka hler, C. J., and Michaelis, D. (2008). Tomographic and time resolved piv measurements on a finite cylinder mounted on a flat plate. Experiments in Fluids, 45(4):715–724.

[21]Keane, R. D. and Adrian, R. J. (1992). Theory of cross-correlation analysis of piv images. Applied Scientific Research, 49(3):191–215.

[22]Soria, J. (1996). An investigation of the near wake of a circular cylinder us- ing a video-based digital cross-correlation particle image velocimetry tech- nique. Experimental Thermal and Fluid Science, 12(2):221–233.

[23]Soloff, S. M., Adrian, R. J., and Liu, Z. C. (1997). Distortion compensation for generalized stereoscopic particle image velocimetry. Measurement Science & Technology, 8(12):1441–1454.

[24]Wieneke, B. (2008). Volume self-calibration for 3d particle image velocimetry. Experiments in Fluids, 45:549–556.

[25]Westerweel, J. and Scarano, F. (2005). Universal outlier detection for PIV data. Experiments in Fluids, 39(6):1096 – 1100.

[26]Scarano, F., Poelma, C., and Westerweel, J. (2007). Towards four- dimensional particle image velocimetry. In 7th International Symposium on Particle Image Velocimetry, Rome, Italy.

[27]Worth, N. A., Nickels, T. B., and Swaminathan, N. (2010). A tomographic piv resolution study based on homogeneous isotropic turbulence dns data. Experiments in Fluids, DOI 10.1007/s00348-010-0840-1.

[28]Parker, K., von Ellenrieder, K. D., and Soria, J., "Morphology of the forced oscillatory flow past a finite-span wing at low Reynolds number", *Journal of Fluid Mechanics*, Vol. 571, 2007, pp. 327-357.

[29]Petitjeans, P., and Wesfreid, J-E., "Vortex stretching and filaments" *Applied Scientific Research*, Vol. 57, 1997, pp. 279-290.

3C-3D Velocity Field Measurements of the Wake Region of Low Reynolds Number Flow around a Flat Plate Undergoing Transient Pitch-Ramp Motion

A-J. Buchner*, N. Buchmann*, C. Atkinson* and **J. Soria***

*Laboratory for Turbulence Research in Aerospace and Combustion
School of Mechanical and Aerospace Engineering
Monash University
Melbourne, Australia
e-mail: abel-john.buchner@eng.monash.edu.au, julio.soria@eng.monash.edu.au (corresponding author)

Abstract

Unsteady aerodynamics in the low Reynolds number domain is of great importance to the development of Micro Air Vehicles (MAVs). There exists a deficiency of information on the nature of the three-dimensionality of flow over, and in the wake of, pitching aerofoils. The flow behavior and governing phenomena are not well understood. This paper extends previous two-dimensional (2D) work [1] by taking multi-dimensional (3D), multi-component (3C) measurements using tomographic particle image velocimetry (Tomo-PIV). The three-component, three-dimensional (3C-3D) velocity field in the wake of a flat plate undergoing a pitch-hold-return motion is investigated. The experiments are conducted in a water tunnel at a Reynolds number of 7,500 and a dimensionless pitching rate of $K_c = 0.93$. The focus is on the interaction of the leading edge vortex in the wake of the pitching plate, highlighting the three-dimensional organisation of the vortex structure.

1 Introduction

Studies of high-rate low-Reynolds number unsteady aerodynamics have previously found interest in areas such as helicopter dynamic stall, wind turbines, and aircraft flutter. However, recently the potential to mimic the mechanism of propulsion of birds and insects has led researcher to investigate unsteady low Reynolds number aerodynamics with a view to application in Micro Air Vehicle (MAV) and Unmanned Air Vehicle (UAV). In the past, studies of unsteady flows have been motivated in the main by a desire to avoid or reduce such undesirable effects as flutter, vibrations and gust response [2]. Although there is large amount of literature available on these problems, there remains some disagreement in the applicability of conventional aerodynamic models and for example, the relative importance of coherent structures in the dynamics of these flows. This mainly arises due to the lack of a unified or canonical problem, which makes it difficult to assess the merits of a particular computation or accuracy of an experiment. To overcome this difficulty, a suitable canonical problem is being investigated - a linear pitch-hold-return motion of a flat plate with round edges and an infinite span. At high dimensionless rates and low Reynolds number, this problem is applicable to MAV's, as well as being a 'classical' problem, in the sense that it can be comparable to results in literature.

Flow around a flat plate has been extensively studied. At zero angle of incidence, the wake behind this class of body assumes a symmetrical time-averaged mean pattern, with the instantaneous flow characterised by periodic coherent patterns resulting from vortex shedding [3]. Flow separation occurs at the leading and trailing edges of the plate, with two alternating shear layers of equal strength but opposite sign rolling up into large-scale vortices which are shed into the wake in the form of a vortex street.

Inclining the plate to the free-stream disturbs this symmetry [3]. In an early experimental investigation into the effect of pitch oscillations, it was observed that the oscillation induced an angle of attack, producing a normal force vector with fluctuating thrust and lift components depending on the instantaneous angle of attack [4]. Koochesfahani [5] also studied the flow around infinite-span airfoils undergoing pure pitching motion, observing that at least two asymmetric vortices were produced per pitching cycle, with vortices shed from the leading edge being more diffused, and of lower peak vorticity than an equivalent trailing edge vortex at the same axial location. The massively separated flow over the upper surface of the pitching airfoil allows for the production of large transient peaks of lift at this scale, as described by Parker et al. [4, 6].

This paper builds on the work of Kilany et al. [1, 7] but extends their stereoscopic 3C-2D flow measurements of this phenomenon into a three-dimensional volume domain through the use of tomographic particle image velocimetry (Tomo-PIV) measurements, providing three-component, three-dimensional (3C-3D) velocity fields. In this present work, Tomo-PIV is utilised to extract 3C-3D velocity vector fields of the coherent structures and the dynamics of the wake region of a flat plate undergoing transient pitch-

ramp motion. The experiments were conducted in the horizontal water tunnel at the Laboratory for Turbulence Research for Aerospace and Combustion (LTRAC). The tunnel has 5 test sections, each measuring 500 mm x 500 mm x 1000 mm. The experiments reported here were conducted in the fourth test section downstream of the contraction. The turbulence intensity level in the test section for these experiments is less than 0.1% with a very uniform mean velocity profile across the width of the test section [4, 6].

A pitching carbon fibre flat plate with rounded leading and trailing edges, of 100 millimetre chord and of span equal to that of the 500 millimetre LTRAC water tunnel was pitched about the half-chord point. The motion sequence used was identical to that used by Kilany et al. [1, 7]. The transient ramp-hold-return motion of the flat plate is characterised by a non-dimensional velocity ratio given by $K=c\dot{\theta}/2U_\infty$ where $\dot{\theta}$ is angular velocity of the flat plate which is kept constant during each pitch motion in this study. Measurements were taken at a Reynolds number of Re = 7; 500 and K = 0:93.

The Tomo-PIV technique involved seeding the flow with small glass spheres and a voluminous region of the wake of the pitching airfoil was illuminated using a 532nm dual-cavity New Wave Nd:YAG laser. In contrast to the measurements taken by Kilany et al. [1, 7], only the wake of the airfoil is under consideration in this paper. Four PCO 4000 cameras under an angular configuration of $\pm 30°$ and $\pm 50°$ captured the laser scattered from the seeding particles. By studying the migration of the particles between images at times close to each other, and comparing between images from different perspectives, the instantaneous 3C-3D velocity field in the wake can be measured. The synchronized double single-exposed image pairs by the four cameras are acquired in a phase-triggered sense. Allowing for the phase related spatio-temporal evolution of the 3C-3D velocity and vorticity fields to be studied. Full details of the Tomo-PIV method used in this study are described in Atkinson and Soria [8].

The vortex patterns observed in two dimensions from the stereo-PIV measurements [7] are expected to, in three dimensions display three dimensional flow patterns which affect also the behaviour in two dimensions. Quantitative data based on the 3C-3D Tomo-PIV measurements describing the spatio-temporal evolution of these phenomena will be presented and discussed.

2 Principle of Tomo-PIV

Tomo-PIV is a technique allowing reconstruction of a full 3C-3D instantaneous velocity field and in doing so thus also yields all nine components of the velocity gradient tensor. The process involves reconstruction from three or more camera views (in this case, four) of an illuminated volume in a seeded flow. Triangulating the intensity distributions recorded by each camera allows individual particles to be located in three-dimensional space, a process carried out by the *multiple line of sight - simultaneous multiplicative algebraic reconstruction technique* (MLOS-SMART) algorithm [8]. This algorithm significantly shortens the reconstruction time over the currently ubiquitous Multiplicative Algebraic Reconstruction Technique (MART) algorithm by excluding voxels containing zero return intensity, demonstrated by Figure (1).

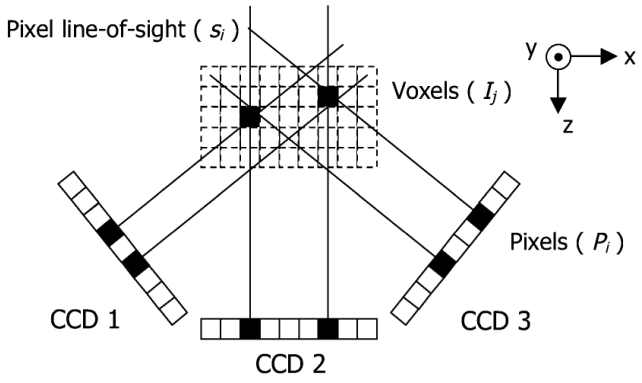

Figure 1: Schematic of the MART technique.

It has been shown that 10-15 particles per interrogation region is sufficient for obtaining a valid displacement vector estimate [9]. The volume fraction of voxels with significant intensity within the reconstruction volume will therefore typically be of the order of only 5%, meaning that approximately 95% of the reconstructed volume will have a negligible intensity and can be excluded from the reconstruction process. (Atkinson and Soria [8] contains details of the algorithm). Following the volume reconstruction, the 3D particle intensity fields are evaluated with a 3D spatial cross-correlation routine [10] to determine the instantaneous 3C-3D velocity fields.

3 Experimental Conditions

3.1 Apparatus

The Monash University horizontal water tunnel facility operated by the Laboratory for Turbulence Research in Aerospace and Combustion (LTRAC) was used for the experiments. The tunnel consists of a 5000mm test section with a 500mm x 500mm square cross-section. The freestream turbulence level is less than 0.1% [6]. The experiments are conducted at approximately the centreline of the tunnel. A carbon fibre flat plate, dimensionally similar to that used by Ol [11], with rounded edges, chord length 100mm, span 470mm and thickness of 2.3mm is used for the current experimental investigation.

The vertically mounted flat plate is driven by a Rorze stepper motor (figure (3)) with a drive resolution of 80,000 steps per revolution to pitch around the half chord point. Control is provided via an in-house Motion Architect AT6400 multi-axis motor controller program. Figure (2) gives an overview of the experimental setup.

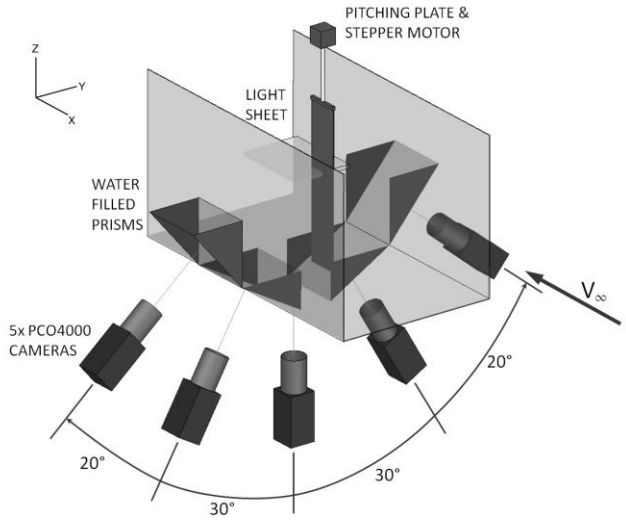

Figure 2: Schematic of the optical arrangement showing the 5 digital cameras, viewing prisms, measurement volume and flat plate geometry

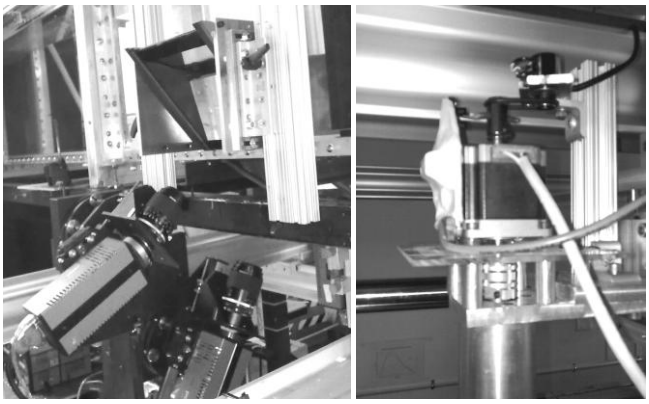

Figure 3: Camera setup and pitching mechanism.

3.2 Pitching Plate Motion Profile

The pitching motion undergone by the plate requires that each cycle the pitch angle changes linearly to a maximum angle of θ=40º, and returns to its zero position after a pause of 0.05 t/T. The entire cycle is completed over a period of T=1second, and then is repeated after a hold period of 20 time periods to allow for flow disturbances to convect downstream. The pitch angle trace of this pitch-hold-return motion is shown in Figure (4).

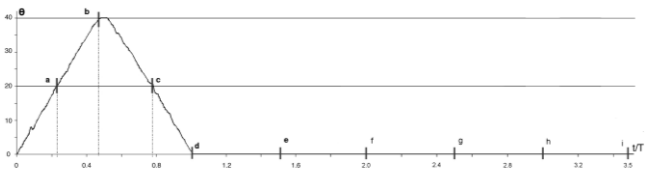

Figure 4: Pitching plate motion profile

The rate at which the plate pitches can be characterised by the non-dimensional velocity ratio (equation 1)

$$K_C = \frac{c\dot{\theta}}{2U_\infty} \quad (1)$$

where $\dot{\theta}$ is the steady angular velocity of the flat plate, U_∞ the free-stream velocity and c the chord length. A summary of the current experimental parameters, which are identical to those used in previous stereoscopic PIV experiments by Kilany et al. [1], is given in Table (1).

Table 1: Experimental Parameters

Parameter	Value
c	100mm
U_∞	75mm/s
θ	0-40º
Re_C	7,500
K_C	0.93

3.3 Optical Arrangement

The imaging equipment consists of five PCO.4000 digital CCD cameras mounted co-radially about an arc at angles of 0º, 30º and 50º (as in Figure (2)). Each camera is equipped with a 105mm focal length lens. As the image plane and subject plane are not parallel, the Scheimpflug condition is invoked to correct the image focus gradient and water filled glass prisms are used to reduce optical refraction effects at the tunnel wall. The cameras are calibrated using the method described by Soloff et al. [12] through a thickness of 12mm, and a maximum calibration error of between 1 and 2 pixels is achieved by applying self calibration [13] for refinement. A comprehensive list of the optical and PIV parameters is included in Table (2).

Table 2: Optical and PIV Parameters

	Parameter	Quantity
Tomo-PIV Setup	Cameras	4008x2672px^2, 16 bit $0, \pm 30, \pm 50$deg
	Laser	Nd:YAG, 240mJ
	Flow Seeding	54μm nylon spheres (ρ=1.01g/cm^3)
Imaging Properties	Magnification	0.26
	Resolution	25 px/mm
	FoV (Sx x Sy x Sz)	3500x2250x350 px^3 130 x 90 x 14 mm^3 1.3 x 0.9 x 0.14c
	Lens Aperture (f#)	11
	Particle image diameter	≈2.3px
	Depth of Field	≈12mm
	Separation time	6ms
	Avg. Displacement	12px

The seeded flow (54μm nylon spheres, ρ = 1.01 g/cm^3) is illuminated using a 240mJ pulsed, dual-cavity Nd:YAG laser. It is focused into a thick light sheet which is truncated through a slit to yield a 12mm thick light sheet with well defined boundaries. The light sheet is aligned lengthwise through the test section of the tunnel, from the downstream direction. The double-shutter exposure delay of 6ms is set to give a freestream average particle displacement of 12 pixels (0.48mm).

4 Data Processing and Analysis

Image preprocessing is required to reduce reconstruction times and provide a more accurate reconstruction. The background intensity is removed, thus increasing the proportion of zero voxels, to take full advantage of the MLOS-SMART algorithm. After background subtraction, band-pass filtering and then Gaussian smoothing are applied to equalize the particle intensities across the image and between cameras.

The MLOS-SMART technique was implemented with 10 iterative corrections, and an initial solution and relaxation parameter of unity. The particle intensity reconstruction volume is 3500 x 2250 x 350 pixel^3 (Table (2)). The reconstructed volumes are cross correlated using an in-house developed multi-grid multi-pass FFT-based cross-correlation algorithm [10] to render the 3C-3D velocity field. An interrogation volume size of 64^3 voxels (=2.56mm^3) with 50% overlap are used to provide velocity fields of 96 x 65 x 9 vectors.

Vector validation is applied in the form of a normalised local median filter [14] and a maximum displacement constraint. Invalid vectors (approx 2-10% of total) are replaced via a mean vector interpolation. Noisy fluctuations in the velocity gradients are suppressed by filtration with a 3 x 3 x 3 Gaussian kernel (σ = 1) [15, 16]. The spatial frequency response remains unaffected due to the equal size of the filter kernel and interrogation window.

5 Results and Discussion

5.1 Flow topology and Spanwise Velocity

Previous studies [1, 7, 11, 17] have shown the two dimensional flow topology to be expected about a pitching plate. This section addresses, not the two-dimensional flow pattern, but the spanwise flow associated with it. It can readily be observed that regions of high vorticity are accompanied by associated spanwise velocity components, and also high gradients of such. This could be indicative of the presence of vortex stretching as described in [18].

The plots of the root mean square (RMS) of the instantaneous spanwise velocity components (Figure (5)) give an indication of the unsteady nature of the flow in the vortex regions and provide insight into the expected magnitude of the spanwise components. Not only are there coherent spanwise velocities, due to vortex stretching, but the amount of variation suggests smaller substructures are at play, including vortex filaments unaligned with the z-axis. This is discussed in more depth in Buchner, et. al. [19].

Of note here is the sequence from t=2.5T to t=3.5T showing the leading edge vortex (LEV) moving into the field of view. The plot relating to the timestep t=3.5T shows another feature which becomes apparent from the RMS plot, an arcing region of spanwise velocity encompassing the upstream portion of the LEV. This region is weaker than those components seen in the vortex core but is coherently defined and suggests a mechanism for spanwise flow separate from the LEV. This is investigated further in later sections.

5.2 Instantaneous Spanwise Flow Patterns

Looking again at the spanwise flow structures in the leading edge vortex, now in an instantaneous sense, more information comes to light. Figure (6) shows the instantaneous spanwise velocities for three timesteps as the LEV convects into the field of view. The black contour lines are lines of constant spanwise velocity (w), and illustrate the true three-dimensional nature of this 'nominally' two-dimensional experiment. The dashed lines represent negative (into page) velocity. They are spaced at intervals of w = 5mm/s.

More detailed discussion on the trailing edge vortices is contained in Buchner, et. al. [19], but here the spanwise substructures within the LEV as it convects downstream of the trailing edge are explored. During the pitching motion cycle the maximum spanwise component of velocity to be expected has been found to be of the order of 10% of the stream velocity [19]. Figure (6a) shows an instantaneous flowfield at t = 2.5T. The leading edge vortex has begun to move into the field of view and, associated with it, are strong spanwise velocity gradients. Most of the region within the leading edge vortex core displays strong spanwise flow, which peaks at approximately 85% of the freestream velocity. It is interesting to note that with phase averaging these regions of strong spanwise flow tend to cancel and so it is observed that the spanwise velocity is not of constant sign over a number of phases. This is the reason for using RMS in the previous section rather than phase averaging.

The spanwise flow within the LEV seems to be more strongly directional than that seen in the trailing edge vortices. The TEV spanwise flow tends to form couplets of opposing sign spanwise flow indicating small areas of unaligned with the z-axis.

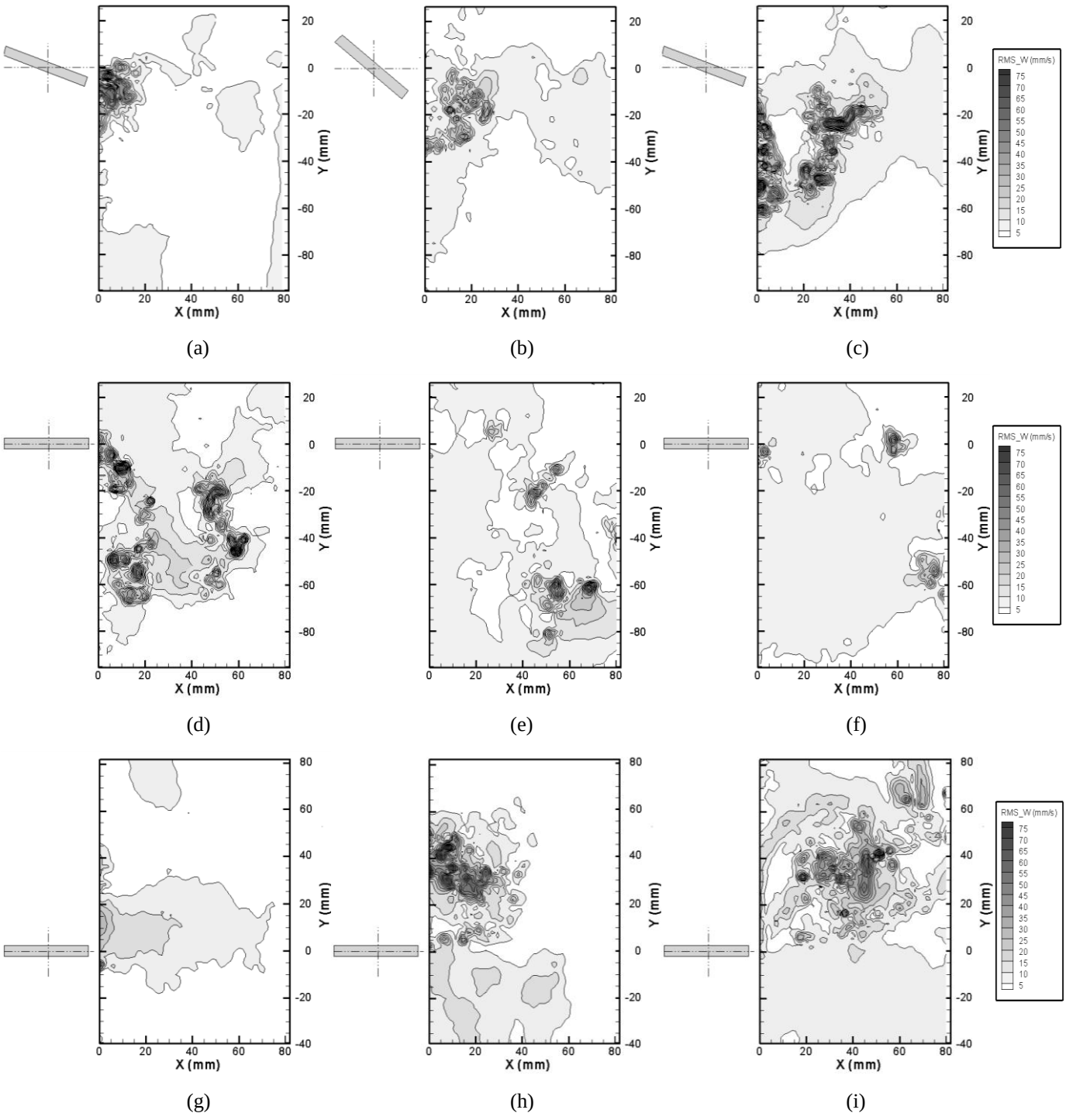

Figure 5: Contour maps of spanwise velocity RMS. (a) t=0.24T; (b) t=0.47T; (c) t=0.77T; (d) t=1.00T; (e) t=1.50T; (f) t=2.00T; (g) t=2.50T; (h) t=3.00T; (i) t=3.50T.

The plots of instantaneous spanwise velocity contours confirm the existence of a structure separate to the LEV causing spanwise velocity (Figure (6c)). In addition to the strong spanwise velocity in the core of the LEV, a small region of weak spanwise velocity is formed just below the LEV. This region is associated with a vortex of opposite sign to the LEV shedding from the trailing edge as a result of the passage of the LEV. More importantly, a long, arcing structure is observed upstream, consisting of two lines of opposite direction spanwise velocity. This confirms the RMS results from section 5.1 and appears to indicate the presence of a distinct vortex filament lying along this path. It should be noted that this feature does not appear in every instantaneous velocity field, but presumably arises from instabilities in the flow separation and occurs in random positions along the span of the plate.

5.3 Structure of the Leading Edge Vortex

Figures (7a-c) show instantaneous isosurfaces of the Q-criterion and are shaded by spanwise velocity. The three figures demonstrate the evolution of the LEV topology downstream of the trailing edge. Figure (7a) has the LEV moving into the field of view and the Karman Street from the trailing edge can be clearly seen also. Figure (7b) shows the LEV continue to move into frame whilst the spanwise components of velocity intensify. The effect of the LEV on the trailing edge Karman Street is now readily apparent.

The next time step (figure (7c)) presents some interesting insight into the flow behavior. At t = 3.5T the LEV has moved fully into the field of view. There are also two regions of vorticity to the left of the figure, as indicated by the Q criterion isosurfaces. These correspond with the features described in the previous sections, relating to spanwise flow structures in these positions in figures (5i) and (6c). The one nearest the LEV is a region of vorticity opposite in sign to the LEV, shed from the trailing edge in response to the passage of the LEV. The left-most structure is however more interesting. It is a vortex filament not aligned with the z-axis, but rather being stretched tangentially about the LEV.

This type of structure has been previously observed computationally in Garmann and Visbal [20]. It finds that, accompanying leading edge vortex separation from the upper surface of a pitching plate, is a tendency for the flow to form complicated streamwise vortex tendrils. These can be seen forming at τ=3-4 in figure (8). Figure (7c) can now provide supporting experimental evidence for this phenomenon.

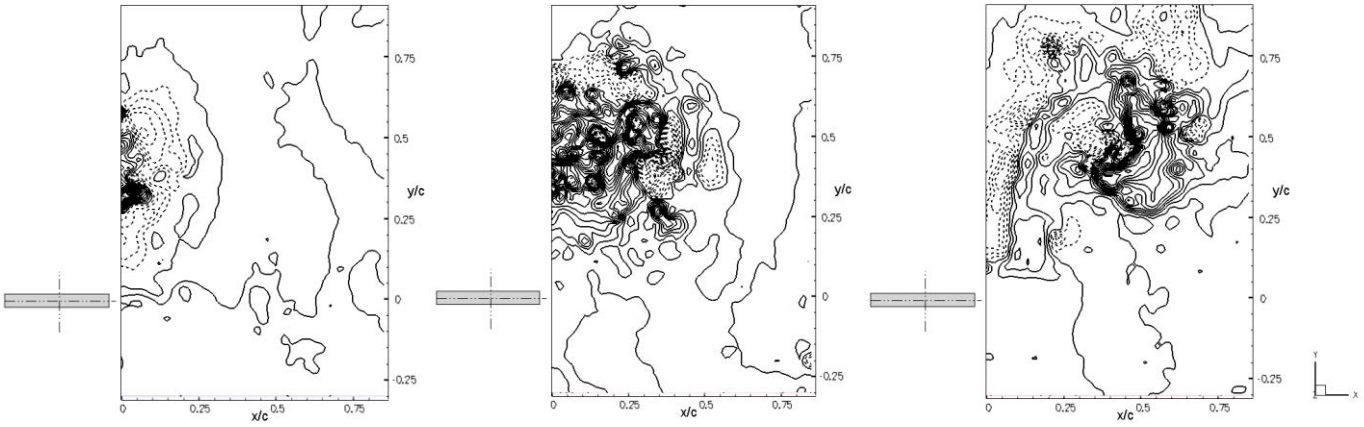

(a) (b) (c)

Figure 6: Instantaneous spanwise velocity components (a) t=2.5T; (b) t=3.0T; (c) t=3.5T.

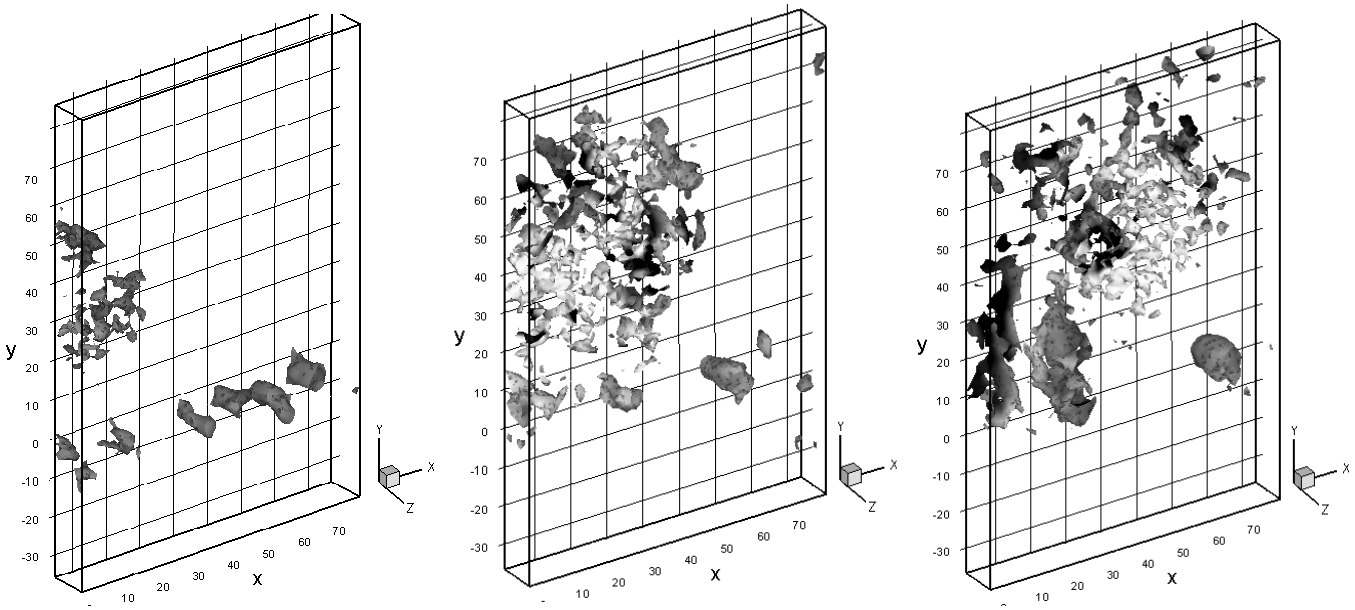

(a) (b) (c)

Figure 7: Instantaneous 3C-3D flowfields showing isosurfaces of Q criterion, shaded by spanwise velocity. (a) t=2.50T; (b) t=3.00T; (c) t=3.50T.

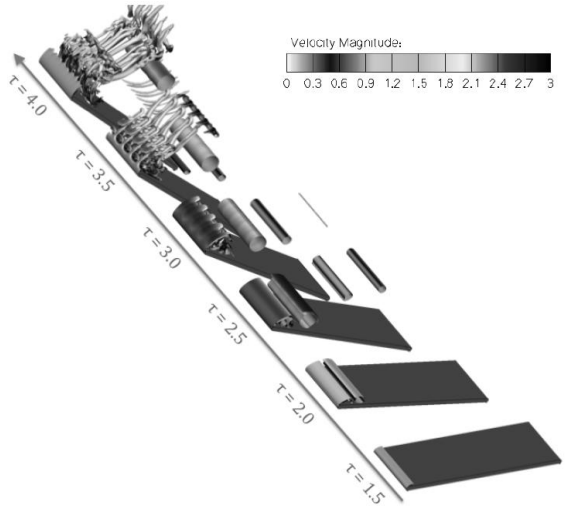

Figure 8: LES numerical data taken from Garmann and Visbal [20] illustrating 3D flow topology

6 Concluding Remarks

Although the two-dimensional flow over a pitching plate has been studied extensively, little is known about the three dimensional behavior of such a flow. Recent computational work [20] has shown that complicated interactions in the flow cause the formation of streamwise vortex filaments even in a nominally two-dimensional case. There is however very little experimental data which could be used to verify these results.

The application of Tomographic PIV allows instantaneous realization of a flowfield over a three-dimensional domain and thus provides an opportunity to investigate the aforementioned structures experimentally and provide supporting evidence for any computational work.

The study carried out in this paper provides evidence for the structures shown to exist in Garmann and Visbal [20]. In addition, significant spanwise flows have been observed within the leading and trailing edge vortices shed from a pitching plate in low Reynolds flow. Though in each instantaneous realization the spanwise velocity components in any particular vortex tend to favour one direction, indicating vortex stretching, this direction is non-constant over a number of cycles. For this reason, a phase average will not yield insight into the spanwise flow. Instead, the root mean square was taken to quantify the distribution of spanwise velocity magnitude. Spanwise velocity was found to peak in the leading edge vortex at a magnitude approaching that of the freestream.

Of interest is the variation in spanwise velocity within each vortex structure. In many cases it is observed that spanwise flow tends to form in small couplets with regions of spanwise flow in the opposite direction, a trend which strengthens as the trailing edge vortices convect downstream and become more disparate [19]. This phenomenon suggests the presence of small vortex filaments unaligned with the z-axis.

7 Acknowledgements

This material is based on research sponsored by the Air Force Research Laboratory, under grant number FA2386-09-1-4091. The U.S. Government is authorized to reproduce and distribute reprints for Governmental purposes notwithstanding any copyright notation thereon.

References

[1] Kilany K., Judde, C., and Soria, S., Multi-component, Multi-dimensional PIV Measurements of Low Reynolds Number Flow Around Flat Plate Undergoing Pitch-Ramp Motion, *39th AIAA Fluid Dynamics Conference*, San Antonio, Texas, 2009.

[2] McCroskey, W. J., Unsteady airfoils. *Annual Review of Fluid Mechanics*, **14**, 1982, 285 – 311.

[3] Lam, K. M., and Leung, M. Y. H., Asymmetric vortex shedding flow past an inclined flat plate at high incidence, *European Journal of Mechanics B/Fluids*, **24**, 2005, 33-48.

[4] Parker, K., von Ellenrieder, K. D., and Soria, J., Morphology of the forced oscillatory flow past a finite-span wing at low Reynolds number, *Journal of Fluid Mechanics*, **571**, 2007, 327-357.

[5] Koochesfahani, M. M., Vortical patterns in the wake of an oscillating airfoil, *AIAA Journal*, **27**, 1989, 1200-1205.

[6] Parker, K., von Ellenrieder, K. D., and Soria, J., Using stereo multigrid DPIV (SMDPIV) measurements to investigate the vortical skeleton behind a finite-span flapping wing, *Experiments in Fluids*, **39**, 2005, 281-298.

[7] Kilany K., Judde C., Ol M. V., and Soria J., Application of stereoscopic piv to a pitch- ramp problem in low Reynolds number flow. *8th International Symposium on Particle Image Velocimetry*, Melbourne, Australia, 2009.

[8] Atkinson, C. and Soria, J., An efficient simultaneous reconstruction technique for tomographic particle image velocimetry. *Experiments in Fluids*, **47(4)**, 2009, 553-568.

[9] Keane, R. D. and Adrian, R. J., Theory of cross-correlation analysis of piv images. *Applied Scientific Research*, **49(3)**, 1992, 191-215.

[10] Soria, J., An investigation of the near wake of a circular cylinder using a video-based digital cross-correlation particle image velocimetry technique. *Experimental Thermal and Fluid Science*, **12(2)**, 1996, 221-233.

[11] Ol, M.V., The High-Frequency, High-Amplitude Pitch Problem: Airfoils, Plates and Wings, *39th AIAA Fluid Dynamics Conference*, San Antonio, Texas, 2009.

[12] Soloff, S. M., Adrian, R. J., and Liu, Z. C., Distortion compensation for generalized stereoscopic particle image velocimetry. *Measurement Science and Technology*, **8(12)**, 1997, 1441-1454.

[13] Wieneke, B., Volume self-calibration for 3d particle image velocimetry. *Experiments in Fluids*, **45**, 2008, 549-556.

[14] Westerweel, J. and Scarano, F., Universal outlier detection for PIV data. *Experiments in Fluids*, **39(6)**, 2005, 1096 - 1100.

[15] Scarano, F., Poelma, C., and Westerweel, J., Towards four-dimensional particle image velocimetry. *7th International Symposium on Particle Image Velocimetry*, Rome, Italy, 2007.

[16] Worth, N. A., Nickels, T. B., and Swaminathan, N., A tomographic piv resolution study based on homogeneous isotropic turbulence DNS data. *Experiments in Fluids*, DOI 10.1007/s00348-010-0840-1, 2010.

[17] Eldredge, J. D., Chengjie, W., and Ol, M. V., A computational study of a canonical pitch-up, pitch-down wing maneuver, *39th AIAA Fluid Dynamics Conference*, San Antonio, Texas, 2009.

[18] Petitjeans, P., and Wesfreid, J-E., Vortex stretching and filaments. *Applied Scientific Research*, **57**, 1997, 279-290.

[19] Buchner A-J., Buchmann, N. A., and Soria, J., Wake Measurements of a Pitching Plate using Multi-component, Multi-dimensional PIV Techniques. *17th Australasian Fluid Mechanics Conference*, Auckland, New Zealand, Accepted.

[20] Garmann, D. J, and Visbal, M. R., Implicit LES Computations for a Rapidly Pitching Plate. *40th AIAA Fluid Dynamics Conference*, Chicago, Illinois, 2010.

17th Australasian Fluid Mechanics Conference
Auckland, New Zealand
5-9 December 2010

Wake Measurements of a Pitching Plate using Multi-component, Multi-dimensional PIV Techniques

A-J. Buchner[1], N. A. Buchmann[1] and J. Soria[1]

[1]Laboratory for Turbulence Research in Aerospace and Combustion (LTRAC)
Department of Mechanical and Aerospace Engineering
Monash University, Victoria 3168, Australia

Abstract

Unsteady aerodynamics in the low Reynolds number domain is of great importance to the development of Micro Air Vehicles (MAVs). The low Re flow over, and in the wake of, pitching aerofoils is not well understood. This paper extends previous work [11] to multi-dimensional (3D), multi-component (3C) measurements of this phenomenon by using Tomographic Particle Image Velocimetry (Tomo-PIV). The three-component, three-dimensional (3C-3D) velocity fields in the wake of a flat plate undergoing a pitch-hold-return motion is investigated. The experiments are conducted in a water tunnel at a Reynolds number of 7,500 and a dimensionless pitching rate of Kc = 0.93. The evolution of the trailing edge vortices is investigated, highlighting the three-dimensional organisation of the coherent vortex structure.

Introduction

This paper presents the results of an experimental investigation into the low Reynolds number flow in the wake of a rapidly pitching flat plate with rounded leading and trailing edges. By applying tomographic PIV to a canonical pitch-hold-return problem, the three dimensional topological evolution of the wake can be studied in the context of already existing two-dimensional data. Understanding of the nature of such flows has application in the design of biomimetic inspired micro air vehicles (MAVs) and builds upon the more traditional work done in unsteady and transient flows over foils which has in the past been mainly focussed on the higher Reynolds number regime with application to dynamic stall, manouvre and gust response. Previous work [1, 16, 22, 6] has concluded that at low Reynolds it becomes necessary to use separation induced leading edge vortices in the production of lift and thrust. By combining pitching and heaving motions the desired vortices, and hence forces, can thus be produced.

Conventional aerodynamic models do not easily account for the phenomena observed in low Reynolds number transient flows, and only basic knowledge of the physics involved exists at this time. Early experiments investigating the effect of time varying pitching motion reported the production of a normal force vector with fluctuating thrust and lift components depending on the instantaneous angle of attack [1]. More recent studies by Eldredge et. al. [6] have investigated the sensitivity of leading and trailing edge vortex structures to variations in pitch pivot point, and pitch rate. The former was found to have a significant effect mainly on the formation of the leading edge vortex and its size while the latter tends to produce a tighter leading edge vortex if increased. For higher dimensionless pitch rates, a counter-rotating vortex pair dominates the trailing edge vortex structure whilst at lower rates the flow field tends to exhibit a stream of smaller vortices with less domination by any particular structures. Both the trail of smaller vortices, and the larger counter-rotating pair were also observed in the stereoscopic PIV investigation of Kilany et.al. [11]. Under these conditions the leading edge vortex has a tendency to be more diffused and of lower peak vorticity than an equivalent vortex produced at the trailing edge at the same axial location [12]. The current set of results correlates well with those already published on 2D data, whilst extending the work to look more in-depth at the 3D effects expected within the vortical wake structures.

Principle of Tomographic PIV

The tomographic PIV technique allows the reconstruction of a 3C-3D velocity field, and thus also yields all nine components of the velocity gradient tensor. A volume of the seeded flow is illuminated by means of a thick light sheet, and the intensity distribution is recorded by three or more cameras (in this case, four). Triangulating the intensity distributions recorded by each camera allows individual particles to be located in three-dimensional space, a process is carried out by the Multiple Line of Sight Simultaneous Multiplicative Algebraic Reconstruction Technique (MLOS-SMART) algorithm [3]. The use of this algorthim significantly speeds up the reconstruction process when compared with the currently ubiquitous Multiplicative Algebraic Reconstruction Technique (MART) algorithm by excluding voxels containing zero return intensity. In the same manner as for planar or stereoscopic PIV, the intensity distribution is segmented into interrogation windows, or volumes in the three-dimensional tomographic case, and cross correlated to determine the 3C-3D velocity field.

Proposed by Atkinson and Soria [3], the MLOS-SMART algorithm significantly reduces the computation cost of 3C-3D velocity field reconstruction. The volume fraction of voxels with significant intensity within the reconstruction volume will typically be of the order of only 5% as it has been shown that 10-15 particles per interrogation region is sufficient for obtaining a valid displacement vector estimate [10]. This means that approximately 95% of the reconstructed volume will have a negligible intensity and can be excluded from the reconstruction process, thus reducing computational and data storage requirements (see Atkinson and Soria [3] for more details). Following the volume reconstruction, the 3D particle intensity fields are evaluated with a 3D spatial cross-correlation routine [25] to determine the instantaneous 3C-3D velocity fields.

Experimental Conditions

Apparatus

The Monash University horizontal water tunnel facility operated by the Laboratory for Turbulence Research in Aerospace and Combustion (LTRAC) was used for these experiments. The tunnel has a long, 5000mm, test section with a $500mm \times 500mm$ square cross-section. The freestream turbulence level is less than 0.5%, and the velocity profiles are uniform over the test section by 4000mm from the contraction [16]. This is where the experiments are conducted, at approximately the centreline of the tunnel. A carbon fibre flat plate, dimensionally similar to that used by Ol [14], with rounded edges, chord length 100mm, span 470mm and thickness of 2.3mm is used for the current experimental investigation.

Figure (1c) gives an overview of the experimental setup. The vertically mounted flat plate is driven by a Rorze stepper motor (figure (1b)) with a drive resolution of 80,000 steps per revolution to pitch around the half chord point. The stepper motor is controlled by an in-house program for a Motion Architect AT6400 multi-axis motor controller.

Optical Arrangement

The imaging equipment consists of five PCO.4000 digital CCD

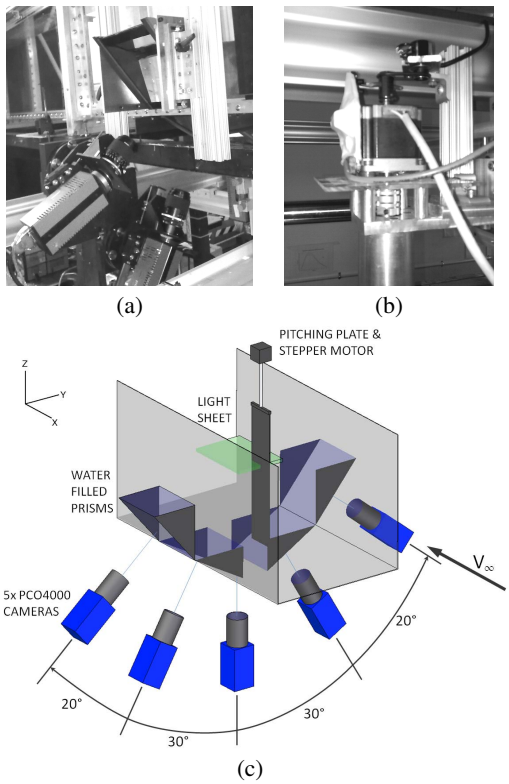

Figure 1: **Experimental Setup:** (a-b) Details of the camera setup and pitching mechanism; (c) Schematic of the optical arrangement showing the 5 digital cameras, viewing prisms, measurement volume and flat plate geometry.

cameras mounted co-radially about an arc at angles of 0, 30 and 50 (as in Figure (1c)). Each camera is equipped with a 105mm focal length lens. Optical refraction effects are minimised through the use of water filled glass prisms. As the image plane and subject plane are not parallel, the Scheimpflug condition is invoked to correct the image focus gradient. The cameras are calibrated using the method described by Soloff et al. [23] through a thickness of 12mm and the resulting calibration error of approximately 10 pixels is reduced via self calibration [27] to between 1-2 pixel. A more detailed description of the tomographic PIV parameters is given in Table (1).

A 240mJ pulsed, dual-cavity Nd:YAG laser is used to illuminate the seeded flow (54m nylon spheres, ρ = 1.01 g/cm3). It is focussed into a thick light sheet which is truncated through a slit to yeild a 12mm thick light sheet with well defined boundaries. The lightsheet is shone lengthwise through the test section of the tunnel, from the downstream direction. The double-shutter exposure delay of 6ms is set to give a freestream average particle displacement of 12 pixel (0.48mm). The thick laser sheet minimises through-plane velocity reconstruction errors as less particles are lost or gained to the lightsheet during the eposure delay.

Pitching Plate Motion Profile

Each cycle, the plate pitches linearly to a maximum angle of $\theta = 40$, holds for 0.05 t/T, and returns to its zero position. This is repeated after a pause of 20 time periods (T = 1sec). The transient pitch-hold-return motion of the flat plate is shown in Figure (2) and characterised by the non-dimensional velocity ratio:

$$K_c = \frac{c\dot{\theta}}{2U_\infty} \tag{1}$$

where $\dot{\theta}$ is the constant angular velocity of the flat plate, U_∞ the free-stream velocity and c the chord length. The Reynolds number is defined as $Re = \frac{U_\infty c}{\nu}$. A summary of the current experimental parameters, which are identical to those used in previous stereoscopic PIV experiments by Kilany et al. [11], is given in Table (2).

	Parameter	Quantity
Tomo-PIV Setup	Cameras	$4008 \times 2672 px^2, 16 bit$
		$0, \pm 30, \pm 50$deg
	Laser	Nd:YAG, $240mJ$
	Flow Seeding	$54m$ nylon spheres, $(\rho = 1.01 g/cm^3)$
Imaging Properties	Magnification	0.26
	Resolution	$25 px/mm$
	$FoV(Sx \times Sy \times Sz)$	$3500 \times 2250 \times 350 px^3$
		$130 \times 90 \times 14 mm^3$
		$1.3 \times 0.9 \times 0.14c$
	Lens aperture $(f\#)$	11
	Particle image diam.	$\approx 2.3 px$
	Depth of field	$\approx 12 mm$
	Separation time	$5ms$
	Max. Displacement	$12 px$

Table 1: Parameters of the Tomo-PIV system

Parameter	Value
c	$100mm$
U_∞	$75mm/s$
θ	$0 - 40deg$
Re	$7,500$
K_c	0.93

Table 2: Experimental parameters

Data Processing and Analysis

To take full advantage of the MLOS-SMART algorithm, it is desired that the background intensity is removed to increase the number of zero-voxels. Background subtraction, band-pass filtering and then Gaussian smoothing are applied to help equalize the particle intensities across the image and between cameras. Volume reconstruction is performed with 10 iterative corrections of the MLOS-SMART technique and an initial solution and relaxation parameter of unity. The volume over which the particle intensities are reconstructed and cross-correlated is $3500 \times 2250 \times 350 pixel^3$ (table (1)).

The velocity fields are calculated with an in-house developed multigrid multi-pass FFT-based cross-correlation algorithm [25]. Interrogation volumes of 64^3 voxels (= 2.56mm) with 50% overlap are used to provide fields of $98 \times 65 \times 9$ vectors. A normalised local median filter [26] and a maximum displacement constraint are used to validate vectors and a maximum displacement limit.

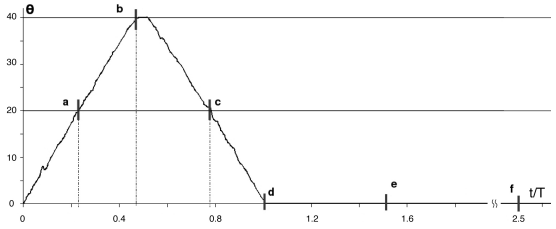

Figure 2: **Measured pitch angle of the flat plate as a function of t/T, with flowfield acquisition points marked.** (a) t/T = 0.24, (b) t/T = 0.47, (c) t/T = 0.77, (d) t/T = 1.0, (e) t/T = 1.5, (f) t/T = 2.5 with T = 1sec.

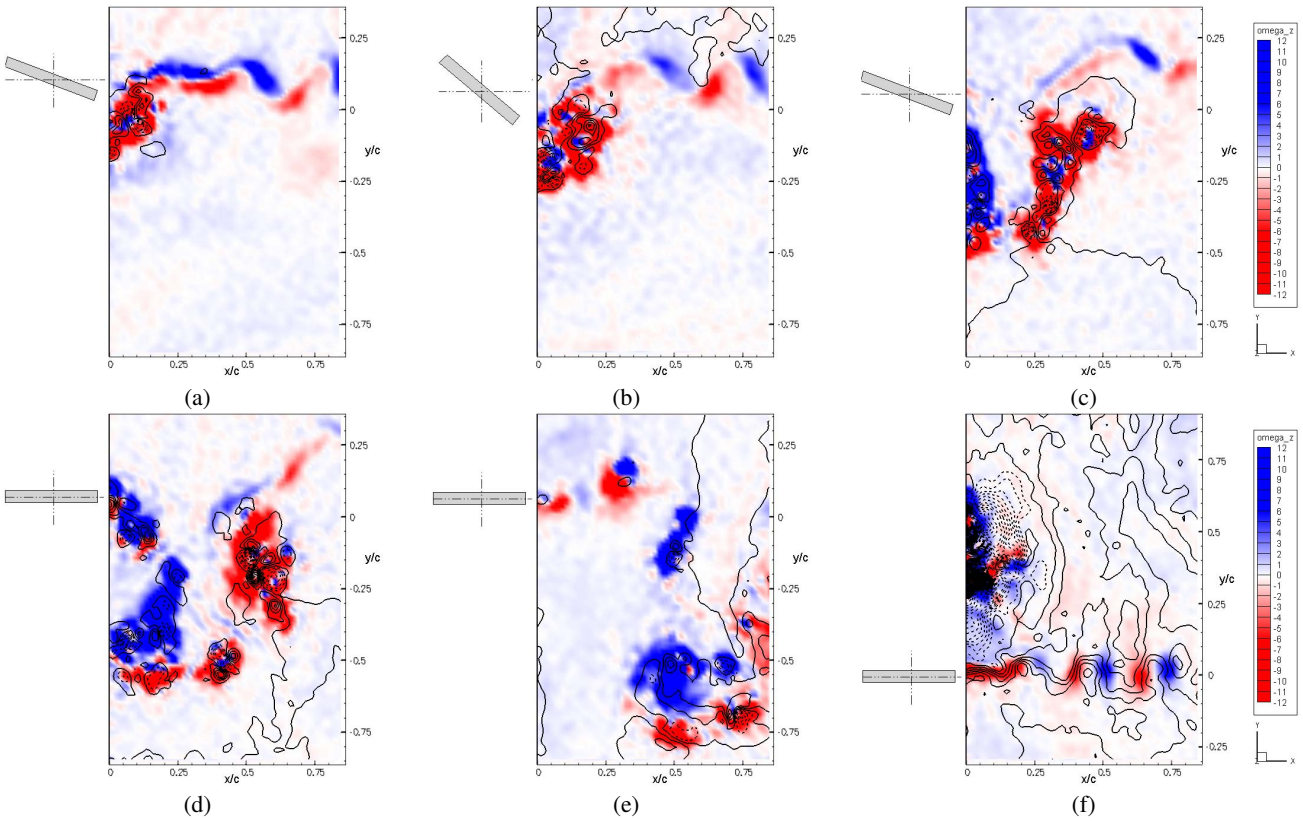

Figure 3: **Instantaneous 3C-3D spanwise vorticity and spanwise velocity fields:** (a) t/T = 0.24, (b) t/T = 0.47, (c) t/T = 0.77, (d) t/T = 1.0, (e) t/T = 1.5, (f) t/T = 2.5.

Invalid vectors (approx 2% of total) are replaced via a mean vector interpolation. For visual representation of the data, the velocity fields are filtered with a $3 \times 3 \times 3$ Gaussian kernel ($\sigma = 1$) to suppress noise fluctuations in the velocity gradients [20, 29]. As the filter kernel is equal to the interrogation window size, the spatial frequency response remains unaffected.

Results and Discussion

The instantaneous flowfields in figure (3) demonstrate the instantaneous flow structure in the wake of the pitching plate. Significant regions of circulation are shed during both the pitch, and reverse, motions and convect downstream at roughly the velocity of the freestream. These regions are indicated in the figure by blue and red shading, denoting vorticity of opposing sign. The overlaid black contour lines are lines of constant spanwise velocity (w), and illustrate the true three-dimensional nature of this 'nominally' two-dimensional experiment. The dashed lines represent negative (into page) velocity. They are spaced at intervals of $w = 2mm/s$.

At t/T = 0.24 (figure (3a)), circulation has begun to be produced by the angular acceleration from a standstill of the plate trailing edge. The circulation produced convects downstream and is replaced by circulation of the opposite sign produced by the plate as it pitches back to its resting position. The evolution of these vortex structures as they move away from the trailing edge is complex. In the phase averages, it is clear that what are initially well structured strings of vortex filaments begin to coalesce into more disparate counter-rotating vortex pairs as they move downstream. Though the length of this paper prohibits the publication of phase averaged plots, this effect can be seen quite clearly in the evolution of the instantaneous fields from figure (3c-d) to figure (3e). The topology of these flows compares well with previously published data [11, 14]. The leading edge vortex does not enter the field of view until approximately t/T = 2.5. This vortex is of significantly larger size than the vortices produced at the trailing edge.

It can readily be observed that regions of high vorticity are accompanied by associated spanwise velocity components, and also high gradients of such. This could be indicative of the presence of vortex stretching as described in [18]. The spanwise velocities are apparent right from the point of circulation production, at the trailing edge, but become more concentrated with time and convection downstream until the magnitude of spanwise flow drops off by $t = 1.5T$. During the pitching motion cycle the maximum spanwise component to be expected is of the order of 10% of the stream velocity. Figure (3f) shows an instantaneous flowfield at $t = 2.5T$. The leading edge vortex has begun to move into the field of view and, associated with it, are strong spanwise velocity gradients. Most of the region within the leading edge vortex core displays strong spanwise flow, which peaks at approximately 85% of the freestream velocity. It is interesting to note that with phase averaging these regions of strong spanwise flow tend to cancel and so it is observed that the spanwise velocity is not of constant sign over a number of phases.

Concluding remarks

Investigations to date such as Parker et. al. [15] show the three-dimensionality of flows past a finite span pitching aerofoil, but fail to address the existence of three-dimensional structures within the unsteady vortex sheet produced by a nominally infinite oscillating aerofoil. In employing tomographic PIV techniques to this problem, these flows were shown to contain significant spanwise axial flow components indicative of the presence of vortex stretching, as described in Petitjeans and Wesfried [18]. The 3C-3D flow fields provided by the tomographic PIV methods in the present study show this phenomenon qualitatively as well as quantitatively, and provide the basis for further investigations into the substructure of the vortex filaments.

Acknowledgments

This material is based on research sponsored by the Air Force Research Laboratory, under grant number FA2386-09-1-4091. The U.S. Government is authorized to reproduce and distribute reprints for Governmental purposes notwithstanding any copyright notation thereon.

References

[1] Anderson, J. M., Streitlien, K., Barrett, D. S., and Triantafyllou, M. S., Oscillating foils of high propulsive efficiency, *Journal of Fluid Mechanics*, **360**, 1998, 41-72.

[2] Arroyo, M. P. and Hinsch, K. D., Recent developments of piv towards 3d measurements. In Schröder, A. and Willert, C., editors, *Particle Image Velocimetry: New Developments and Recent Applications*. Springer-Verlag Berlin-Heidelberg, 2008.

[3] Atkinson, C. and Soria, J., An efficient simultaneous reconstruction technique for tomographic particle image velocimetry. *Experiments in Fluids*, **47(4)**, 2009, 553-568.

[4] Atkinson, C. H. and Soria, J., Algebraic reconstruction techniques for tomographic particle image velocimetry. *Proceedings of the 16th Australasian Fluid Mechanics Conference*, Gold Coast, Australia, 2007.

[5] Burgmann, S., Brücker, C., and Schröder, W., Scanning piv measurements of a laminar separation bubble. *Experiments in Fluids*, **41**, 2006, 319-326.

[6] Eldredge, J. D., Chengjie, W., and Ol, M. V., A computational study of a canonical pitch-up, pitch-down wing maneuver, *39th AIAA Fluid Dynamics Conference*, San Antonio, Texas, 2009.

[7] Elsinga, G. E., Scarano, F., Wieneke, B., and van Oudheusden, B. W., Tomographic particle image velocimetry. *Experiments in Fluids*, 2006.

[8] Hain, R., Kähler, C. J., and Michaelis, D., Tomographic and time resolved piv measurements on a finite cylinder mounted on a flat plate. *Experiments in Fluids*, **45(4)**, 2008, 715-724.

[9] Kähler, C. J., Investigation of the spatio-temporal flow structure in the buffer region of a turbulent boundary layer by means of multiplane stereo PIV. *Experiments in Fluids*, **36(1)**, 2004, 114-130.

[10] Keane, R. D. and Adrian, R. J., Theory of cross-correlation analysis of piv images. *Applied Scientific Research*, **49(3)**, 1992, 191-215.

[11] Kilany K., Judde, C., and Soria, S., Multi-component, Multi-dimensional PIV Measurements of Low Reynolds Number Flow Around Flat Plate Undergoing Pitch-Ramp Motion, *39th AIAA Fluid Dynamics Conference*, San Antonio, Texas, 2009.

[12] Koochesfahani, M. M., Vortical patterns in the wake of an oscillating airfoil, *AIAA Journal*, **27**, 1989, 1200-1205.

[13] Lam, K. M., and Leung, M. Y. H., Asymmetric vortex shedding flow past an inclined flat plate at high incidence, *European Journal of Mechanics B/Fluids*, **24**, 2005, 33-48.

[14] Ol, M.V., The High-Frequency, High-Amplitude Pitch Problem: Airfoils, Plates and Wings, *39th AIAA Fluid Dynamics Conference*, San Antonio, Texas, 2009.

[15] Parker, K., von Ellenrieder, K. D., and Soria, J., Morphology of the forced oscillatory flow past a finite-span wing at low Reynolds number, *Journal of Fluid Mechanics*, **571**, 2007, 327-357.

[16] Parker, K., von Ellenrieder, K. D., and Soria, J., Using stereo multigrid DPIV (SMDPIV) measurements to investigate the vortical skeleton behind a finite-span flapping wing, *Experiments in Fluids*, **39**, 2005, 281-298.

[17] Pereira, F., Stuer, H., Graft, E. C., and Gharib, M., Two-frame 3d particle tracking. *Measurement Science and Technology*, **17(7)**, 2006, 1680 - 1692. Particle tracking;Two frame;Defocusing digital particle image velocimetry (DDPIV).

[18] Petitjeans, P., and Wesfreid, J-E., Vortex stretching and filaments. *Applied Scientific Research*, **57**, 1997, 279-290.

[19] Prasad, A. K., and Adrian, R. J., Stereoscopic particle image velocimetry applied to liquid flows. *Experiments in Fluids*, **15**, 1993, 49-60.

[20] Scarano, F., Poelma, C., and Westerweel, J., Towards four-dimensional particle image velocimetry. *7th International Symposium on Particle Image Velocimetry*, Rome, Italy, 2007.

[21] Scarano, F., Elsinga, G., Bocci, E., and van Oudheusden B.W., Investigation of 3D coherent structures in the turbulent cylinder wake using tomo-piv. in:. *13th Int. Symp. on Applications of Laser Techniques to Fluid Mechanics*, Lisbon, Portugal, 2006.

[22] Shyy, W., Lian, Y., Tang, J., Liu, H., Trizila, P., Stanford, B., Bernal, L., Cesnik, C., Friedmann, P., and Ifju, P., Computational aerodynamics of low Reynolds number plunging, pitching and flexible wings for MAV applications, *Acta Mechanica Sinica*, **24**, 2008, 351-373.

[23] Soloff, S. M., Adrian, R. J., and Liu, Z. C., Distortion compensation for generalized stereoscopic particle image velocimetry. *Measurement Science and Technology*, **8(12)**, 1997, 1441-1454.

[24] Soria, J. and Atkinson, C., Towards 3c-3d digital holographic fluid velocity vector field measurement-tomographic digital holographic piv (tomo-hpiv). *Measurement Science and Technology*, **19(7)**, 2008.

[25] Soria, J., An investigation of the near wake of a circular cylinder using a video-based digital cross-correlation particle image velocimetry technique. *Experimental Thermal and Fluid Science*, **12(2)**, 1996, 221-233.

[26] Westerweel, J. and Scarano, F., Universal outlier detection for PIV data. *Experiments in Fluids*, **39(6)**, 2005, 1096 - 1100.

[27] Wieneke, B., Volume self-calibration for 3d particle image velocimetry. *Experiments in Fluids*, **45**, 2008, 549-556.

[28] Willert, C. E. and Gharib, M., Three-dimensional particle imaging with a single camera. *Experiments in Fluids*, **12(6)**, 1992, 353-358.

[29] Worth, N. A., Nickels, T. B., and Swaminathan, N., A tomographic piv resolution study based on homogeneous isotropic turbulence DNS data. *Experiments in Fluids*, DOI 10.1007/s00348-010-0840-1, 2010.